Journal of Structural Geology 184 (2024) 105158

Contents lists available at ScienceDirect

Journal of Structural Geology

journal homepage: www.elsevier.com/locate/jsg

Quantifying fault interpretation uncertainties and their impact on fault seal and seismic hazard analysis

Billy J. Andrews [a,*], Zoë K. Mildon [a], Christopher A.L. Jackson [b], Clare E. Bond [c]

[a] School of Geography, Earth and Environmental Sciences, University of Plymouth, Drake Circus, Plymouth, PL4 8AA, UK
[b] Department of Earth Science & Engineering, Imperial College, Prince Consort Road, London, SW7 2BP, UK
[c] Department of Geology and Geophysics, School of Geoscience, Meston Building, Aberdeen University, Aberdeen, AB24 3UE, UK

ARTICLE INFO

Keywords:
Bias
Seismic reflection
Displacement analysis
Faults

ABSTRACT

Fault-horizon cut-off data extracted from seismic reflection datasets are used to study normal fault geometry, displacement distribution, and growth history. We assess the influence of three seismic interpretation factors (repeatability, measurement obliquity, and fault cut-off type) on fault parameter uncertainty. Two repeat interpretations resulted in mean differences of 5–15% for throw, 11–42% for heave, 9–31% for displacement, and 7–27% for dip across faults. Measurement obliquity, where faults are interpreted using non-perpendicular transects to fault strike, show increasing uncertainty with increasing obliquity. Uncertainty in throw is 14–24% at obliquities >20° and 6–13% where obliquities <20°. Continuous cut-offs, including non-discrete deformation, generally exhibit greater uncertainties compared to discontinuous (discrete) cut-offs. We consider the effect of interpretation factors on fault parameters used in seismic hazard assessment (SHA) and fault seal, using the established Shale Gouge Ratio (SGR). Even modest measurement obliquities and repeatability errors can affect inputs for SHA, causing large differences in throw- or slip-rate and inferred fault length. Measurement obliquity and repeatability have a variable impact on SGR calculations, highlighting the additional importance of sedimentary layer thickness and distribution. Our findings raise questions about the optimum workflow used to interpret faults and how uncertainties in fault interpretation are constrained and reported.

1. Introduction

The measurement of horizon-fault cut-offs from seismic reflection datasets enables extraction of key fault properties such as heave, throw and fault dip. Analysis of these properties have advanced our understanding of fault geometry and evolution (e.g., Nicol et al., 2005; Jackson and Rotevatn, 2013; Pan et al., 2021; Roche et al., 2021; Rodríguez-Salgado et al., 2023), strain rate and its evolution in active and inactive rift systems (e.g., Meyer et al., 2002; Cowie et al., 2005; Marsh et al., 2010); and fluid-flow properties of faults within hydrocarbon and/or CO_2 reservoirs (e.g.,Yielding, 2002; Gibson and Bentham, 2003; Yielding et al., 2011; Miocic et al., 2014). The use of horizon-fault cut-off data, combined with well data, is routinely used to infer the sealing potential of faults cutting these reservoirs. This is of particular importance for CO_2 storage projects (Klusman, 2003; Amonette et al., 2010), where "appropriately selected and managed schemes" are expected to retain 99% of injected CO_2 over a time period of 1000 years (IPCC, 2005). Fault cut-off data can also be used to infer key parameters (e.g., slip-rate) to feed into fault based seismic hazard assessments (e.g., fault dip, geological slip rate) (Nicol et al., 2005). Nucular waste disposal sites require geologically stable subsurface locations, and hence must be subject to detailed seismic hazard assessment (Fenton et al., 2006; Connor et al., 2009; Mörner, 2013). Where seismic data is involved in this assessment, any uncertainty in horizon cut-off's at faults could lead to uncertainties in the expected hazard at the site and therefore its suitability for storing nuclear waste. It is therefore imperitive to have confidence in conclusions drawn from the analysis of fault properties extracted from seismic reflection datasets and therefore, the uncertainties and biases associated with extraction of underpinning data.

Uncertainties can be broadly classified as objective and subjective (Frodeman, 1995; Tannert et al., 2007; Bond, 2015). Objective uncertainty, also known as "stochastic uncertainty", relates to the methods used for data acquisition, analysis, or interpretation of the raw data

* Corresponding author.
E-mail addresses: billy.andrews@plymouth.ac.uk (B.J. Andrews), Zoe.mildon@plymouth.ac.uk (Z.K. Mildon), c.jackson@imperial.ac.uk (C.A.L. Jackson), clare.bond@abdn.ac.uk (C.E. Bond).

https://doi.org/10.1016/j.jsg.2024.105158
Received 1 November 2023; Received in revised form 10 May 2024; Accepted 14 May 2024
Available online 17 May 2024
0191-8141/© 2024 The Authors. Published by Elsevier Ltd. This is an open access article under the CC BY license (http://creativecommons.org/licenses/by/4.0/).

(Tannert et al., 2007; Pérez-Díaz et al., 2020). In the case of seismic reflection data, these include the velocity model used for the conversion between two-way-time to depth (Schaaf and Bond, 2019; Faleide et al., 2021), the effect of compaction of fault properties (Taylor et al., 2008), the spacing of picks during data extraction (Michie et al., 2021; Robledo Carvajal et al., 2023), and whether the throw across a given fault exceeds or falls below the limit of separability (Brown, 2011; Osagiede et al., 2014).

Subjective uncertainties pertain to biases and variability in results caused by the individual analysing the data (Tannert et al., 2007); these include the geological interpretation and its repeatability. Repeatability, which is the ability to replicate the data and interpretations of a study, is recognised as a crucial aspect of any experiment (e.g., Goodman, 2016). Geology, in particular, is susceptible to subjective uncertainty due to incomplete datasets and the lack of consensus within the research community regarding key concepts and research methods (Frodeman, 1995; Bond, 2015; Pérez-Díaz et al., 2020; Steventon et al., 2022; Magee et al., 2023; Robledo Carvajal et al., 2023). For seismic reflection datasets, subjective uncertainties can lead to multiple interpretations being drawn from the same seismic image (e.g., Bond et al., 2007; Alcalde et al., 2017). Previous work has suggested that fault properties extracted from seismic reflection data should have an error associated with them of between ±5% (Magee and Jackson, 2020a) and ±10% (Magee et al., 2023), however, no parametric studies have been undertaken to date to test these essentially qualitative values.

Motivated by the discussion above, this paper considers the impact of two fault interpretation workflow choices: measurement obliquity to fault-strike and interpreted fault cut-off type (continuous, in which the horizon bends into the fault plane and discontinuous in which the horizon cut-offs at faults are sharp; Fig. 1). We also investigate the impact of repeatability in fault interpretation for these workflow choices. Having, considered the individual and compound uncertainties that result from these choices we examine the impact on the fault properties: throw, heave, dip, and displacement; to show the relative impact of each fault interpretation choice on properties that are used in risk and resource assessment.

2. Expected sources of uncertainty in fault interpretation

In this section we summarise the literature and theoretically expected contribution of each workflow choice on the repeatability of fault data extraction.

Interpretation repeatability: The repeatability of measurements from seismic reflection data is influenced by human bias, leading to uncertainties in locating cut-offs (Schaaf and Bond, 2019). The position of cut-offs will be influenced by the interpreted horizon and fault, the interpreted intersection point and any projection of regional dip onto the fault plane. These factors are expanded upon below:

Interpreted horizons (Fig. 2a): Horizons interpretations (picks) are made along prominent reflections, ideally with consistent waveforms (Brown, 2011). Inconsistent waveforms can result in high rugosity horizon picks, and ultimately structure maps. These inconsistent wave forms are attributed to post-acquisition processing or geological features (Chellingsworth et al., 2015). Auto trackers and smoothing algorithms are commonly used to create geologically "reasonable" horizons, with the choice of methods used introducing subjective uncertainty (Brown, 2011; Chellingsworth et al., 2015). Previous studies have shown that horizon picking uncertainties decrease near wells, potentially due to an increase in interpreter confidence as the seismic reflection data is tied to data in the well (Schaaf and Bond, 2019). Conversely, horizon picking uncertainties increase away from wells, especially in areas of low seismic image quality and near faults (Alcalde et al., 2017b; Schaaf and Bond, 2019). The image quality around faults can be affected by the presence of a damage zone, which can vary in width based on fault displacement and the structural position on the fault (Shipton and Cowie, 2003; Childs et al., 2009; Choi et al., 2016). Furthermore, correlating horizons across faults may be challenging due to variations in reflection properties, the presence of footwall degradation (Bilal et al., 2020), and/or changes in seismic stratigraphy in the footwall/hangingwall, and especially when reflectors cannot be traced around fault tips (Bond et al., 2007; Bond, 2015; Chellingsworth et al., 2015). We anticipate increased horizon picking uncertainty for faults with large displacement, at segment boundaries/fault tips, or in locations where footwall degradation has occurred.

Interpreted faults: Uncertainties in fault placement are influenced by the strength of seismic reflector and image quality (Alcalde et al., 2017b; Schaaf and Bond, 2019) (Fig. 2b). Interpretation uncertainty increases in areas with decreased reflector strength (Schaaf and Bond, 2019). Strong seismic reflectors overlying or underlying weak reflectors reduce uncertainty in our interpretation of the latter, and faults that conformed to expected geometries (e.g., matching the regional trend) are more reliably picked (Bond, 2015; Alcalde et al., 2017a; Schaaf and Bond, 2019).

Interpreted horizon-fault intersection (i.e., cut-offs): The way that reflections (interpreted as horizons) intersect with faults, i.e. cut-offs, are open to interpretation and therefore potentially uncertain. This arises, at least partly, from there being two components of fault-related deformation; *discontinuous*, which results from brittle strain accommodated by fault-slip and is imaged seismically by discrete off-set of horizons across a fault; and *continuous*, which relates to folding (i.e., ductile strain) and/or brittle deformation below the resolution of the seismic reflection dataset, in which horizons are imaged in the seismic reflection data as bending into the fault. As such, two types of cut-off can be measured: discontinuous cut-offs, and continuous cut-offs (Fig. 1b), which account for both the discontinuous and continuous components of deformation (Childs et al., 2017; Delogkos et al., 2017, 2020). These cut-offs can then be used to calculate fault throw, heave, dip, and displacement. The inclusion or not of continuous deformation depends on the scientific objective and the nature of the faulting. For example, to derive long-term fault slip-rates the continuous portion of deformation is considered (Lathrop et al., 2021; Pan et al., 2021). In contrast, only the discontinuous portion is required to calculate lithological juxtapositions, shale gouge ratio and ultimately fault transmissivity.

Uncertainties affect cut-off types differently. Discontinuous cut-offs (Fig. 2c), are influenced by uncertainties in the position of the fault plane and horizon. Analysis of fault cut-offs suggests that areas of low image quality are associated with large uncertainty, as seismic image quality generally decreases with depth this also leads to increased uncertainty with depth (Alcalde et al., 2017b; Schaaf and Bond, 2019). Moreover, cut-offs on faults with low displacement near the limit of separability (Magee et al., 2023) and the hanging wall cut-off of large displacement faults, which are deeper and due to additional accommodation space often show changes in seimic stratigraphy compared to the footwall (Alcalde et al., 2017b), are prone to higher uncertainties. Continuous cut-offs require the regional dip of the horizon to be projected onto the fault plane (Fig. 2d). In cases of small-displacement faults where continuous deformation comprises a significant portion of the displacement, the interpreter must choose where the fault intersects the deflected horizon (Faleide et al., 2021; Magee et al., 2023). This introduces uncertainty as there are multiple feasible locations from which to project the horizon onto the fault plane, as well as the position of the fault plane itself (Fig. 2d). Where both types of deformation are present (e.g., fault growth through a mixture of continuous and discontinuous imaged deformation), the position of the fault plane will likely have lower uncertainty, but the interpreter still needs to subjectively determine where the regional dip of horizons transitions into near-fault continuous deformation.

Seismic image quality vertical exaggeration are common factors that influence subjective uncertainties. To minimise their impact in our analysis, horizons at similar depths, with similar resolutions, are selected and a consistent vertical exaggeration (~1:4) is used during fault picking.

Previous studies have focused on the impact of subjective bias on

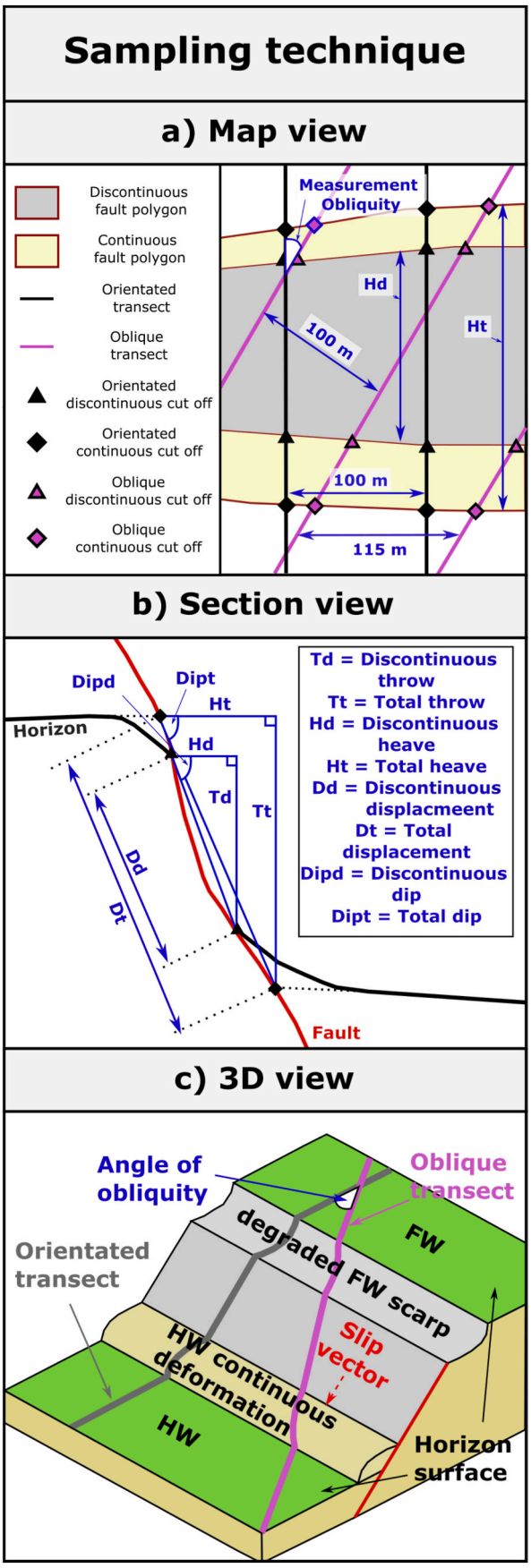

(caption on next column)

Fig. 1. Sample strategy to assess obliquity errors when extracting data from fault cut-offs: a) Map view sample strategy and extracted parameters. Discontinuous and continuous fault polygons represent the horizon gap created by a fault, extending between the hanging wall and footwall for discontinuous and continuous cut-offs, respectively; b) Section view sample strategy and extracted parameters; c) 3D view showing the spatial difference between an orientated and oblique transect.

data extracted from multiple interpreters (Bond et al., 2007, 2012; Bond, 2015; Schaaf and Bond, 2019). However, limited attention has been given to the consistency of an individual's interpretation. Magee et al. (2023) conducted a study where an individual made repeat picks on the same horizon of a low-displacement fault, revealing variations in fault cut-off positions that affected the extraction of throw and heave. Nevertheless, the datasets were found to be statistically equivalent and exhibited lower uncertainty compared to another interpreter's interpretation of the same horizon. Similar 'internal consistency' within individuals interpretations has also been observed in the field classification of faults and fractures (Andrews et al., 2019; Shipton et al., 2020) and seismic reflection-based models (Alcalde and Bond, 2022). This study aims to build on these findings by investigating the magnitude of individual internal consistency in fault properties, examining variations across different horizons, faults, cut-off types and measurement obliquity.

Measurement obliquity: Measurement obliquity is the angle relative to the fault strike that fault and fracture properties are sampled (Fig. 1a), and it can affect the extraction of key properties such as spacing and dip (Terzaghi, 1965; Watkins et al., 2015). Optimal fault interpretation strategies involves sampling using transects that are perpendicular to fault strike. For true normal faults, this is parallel to the slip vector; for all faults measuring fault dip strike perpendicular avoids measuring an apparent fault dip.

The theoretical error on the extracted fault parameters can be estimated by considering the change in cut-off position caused by an oblique sample line (Fig. 3). For a fault with 40° dip, throw errors remain low even at high measurement obliquities (Fig. 3a). However, heave errors exceed 50% at measurement obliquities of ±50° and exceed 10% at an obliquity of ~25°. These errors would lead to moderate over- and underestimates of displacement and dip, respectively, where measurement obliquity exceeds 20° to 30°. Below ~20°, theoretical error estimates suggest that obliquity will have a limited effect on the extraction of fault parameters (Fig. 3). Therefore, we expect measurement obliquity to have a small effect on the extraction of throw (Fig. 3a), but greatly impact measurements of heave (Fig. 3b), and therefore displacement and dip (Fig. 3c and d).

It is not always possible to sample faults using strike perpendicular transects. This is due to the non-linear morphology of faults and the scale-dependant nature of strike. To use strike perpendicular transects along the length of a fault may be time intensive, and the way in which data is combined between different transect orientations could casuse errors in subsequent analysis. Furthermore, if 2D seismic lines are the only available datasets, the lines may not be optimally orientated (i.e., perpendicular) to local fault strike. This study aims to investigate the threshold at which measurement obliquity significantly affects the extraction and interpretation of fault properties, and therefore to provide quantified errors that can be applied to other studies.

3. Dataset and methods

3.1. Seismic data

We use a high-resolution 3D seismic survey (Chandon3D) located on the Exmouth Plateau, offshore NW Australia (Fig. 4). Chandon3D is a time-migrated, zero-phase survey that has a length of 6 s two-way time (TWT) and bin-spacing of 25 m. The data are displayed with a SEG reverse polarity, i.e., a downward increase in acoustic impedance

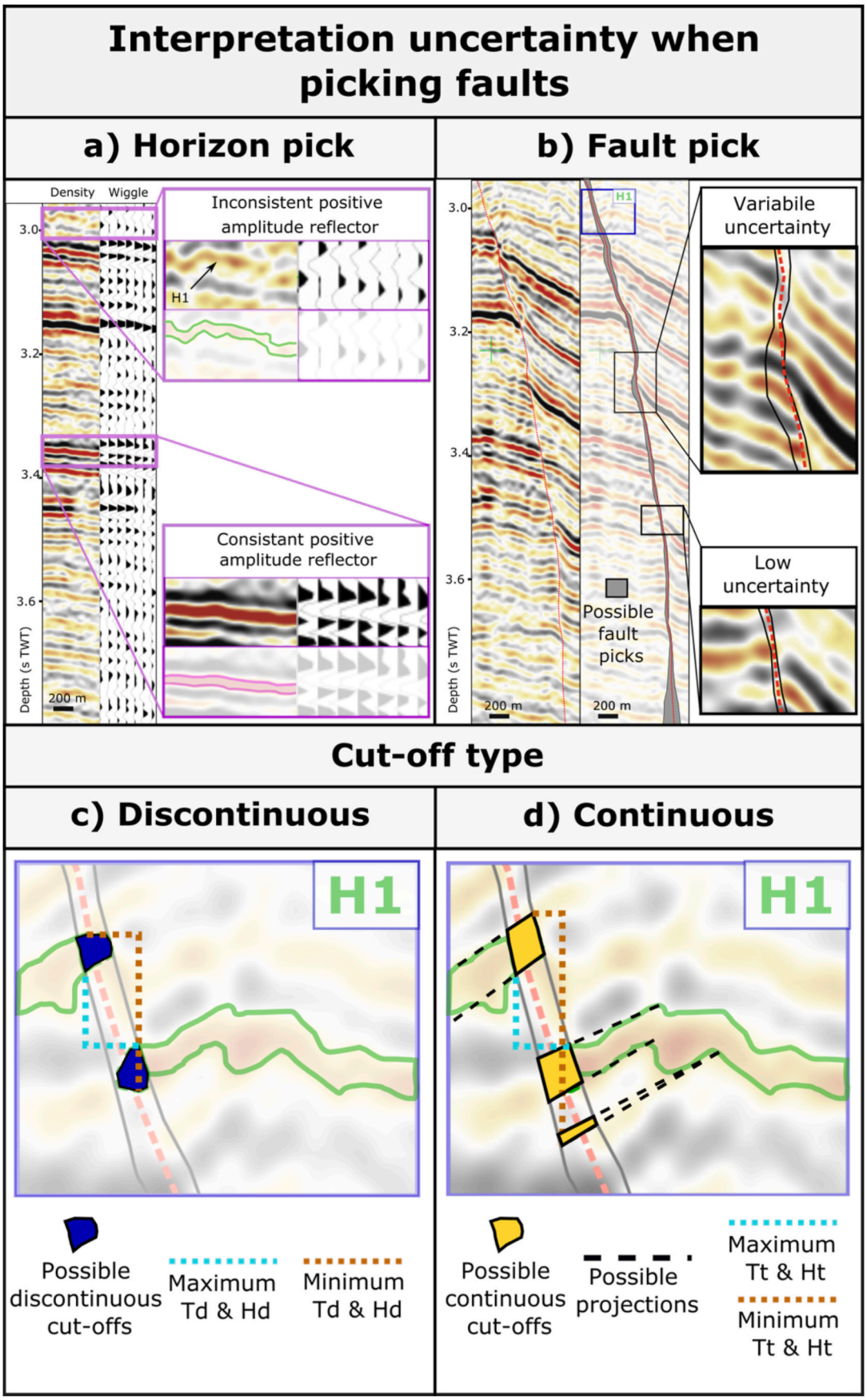

Fig. 2. Examples of expected interpretation uncertainty when picking fault cut-offs; a) quality of reflector used to pick the horizon; b) quality of reflectors close to imaged faults; possible locations of c) discontinuous and d) continuous fault cut-offs caused by uncertainties in horizon and fault picks.

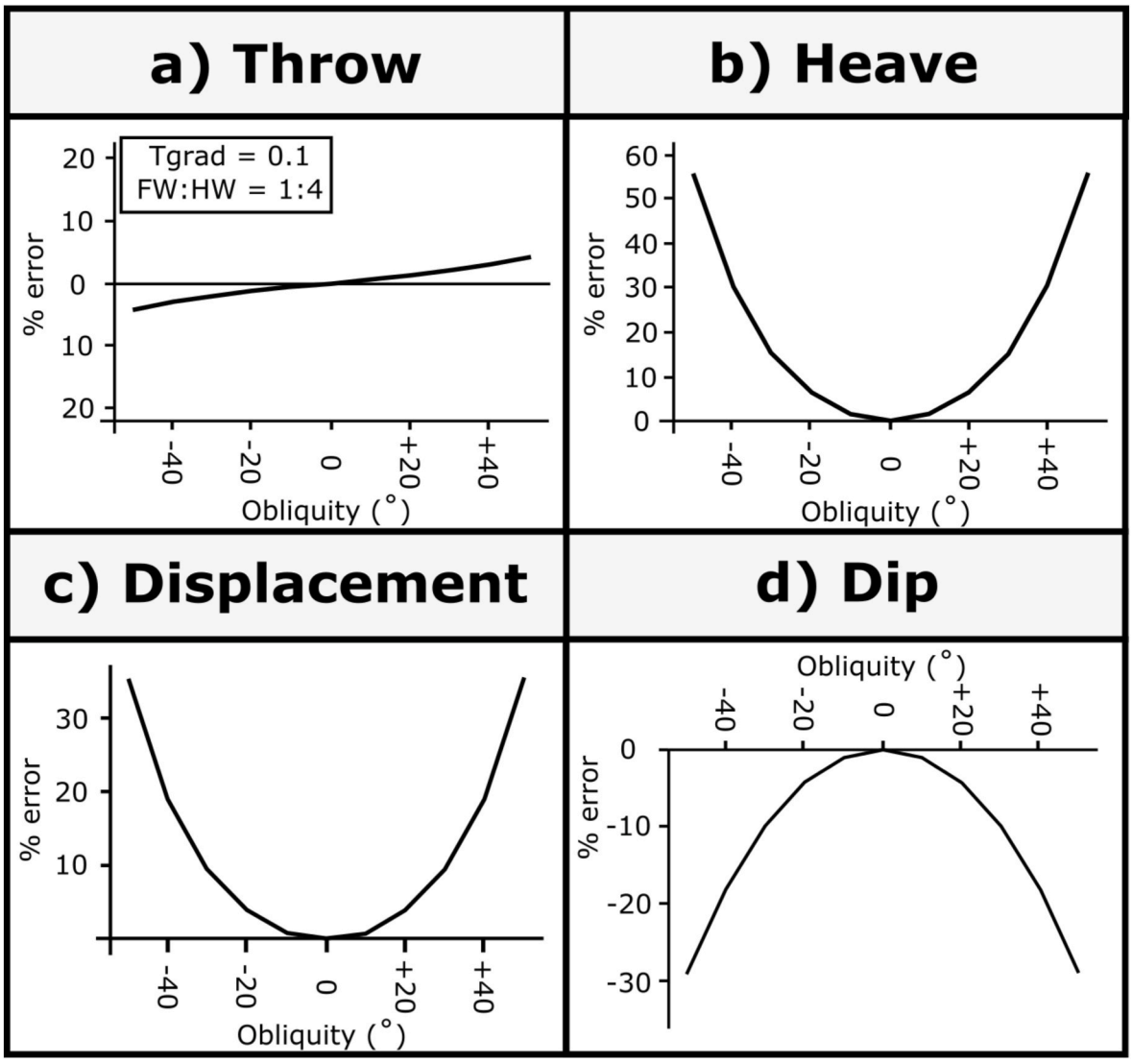

Fig. 3. Theoretical % error across a range of oblique transects for a) throw, b) heave, c) displacement and d) dip assuming a fault dip of 40°. For throw, a throw gradient of 0.1 and a FW:HW displacement ratio of 1:4 was assumed. The shape of the theoretical % error graphs implies that heave, and therefore displacement and dip, will have a high theoretical error at high obliquity, whereas throw will have a lower theoretical error.

corresponds to a trough (black) reflection, and a downward decrease in acoustic impedance corresponds to a peak (red) reflection (Fig. 2a). We used four wells to constrain the age and lithology of the interpreted horizon reflections (Chandon-1, Chandon-2, Chandon-3, Yellowglen).

We estimate seismic velocities using time-depth plots derived from check-shot data obtained from nearby wells (Supplementary 2). Since the interval of interest (~2.9s–4.1s TWT) extends below the depth of the wells (2093 m, 3.324s TWT), we extrapolated seismic velocities through this interval by fitting a second-order polynomial to the combined check-shot dataset. Differences in polynomials between individual wells introduces depth-dependant uncertainty (Supplementary 2); however, given the similar depth of cut-offs across all faults and the moderate-to low-throw magnitude, any absolute errors in depth should be consistent between picks at a given location on the fault. Differences in our analyses are therefore caused by obliquity, fault cut-off choice and interpretation and repeatability errors.

The resolution of an interval of interest in a seismic cube can be estimated by calculating the limits of seperability and visibility respectivey (Brown, 2011). The limit of sperability corresponds to the minimum vertical discance whereby interfaces will prodice two distinct seismic reflectors, and the limit of visibility the vertical distance whereby interfaces are indistinguishable from background noise (Brown, 2011). Between these values, individual reflectors cannot be resolved and they will appear as a tuned reflection package (Brown, 2011) (i.e., no discontinuous deformation will be visible). To calculate the limits of seperability and visibilty, we extract the domant frequencies (f) and average interval velcoities (v) for the shallowest (2.9–3.1 s TWT) and deepest (3.9–4.1 s TWT) intervals analysed in our study. From these we calculate the dominant wavelength (λ) for the interval of interest ($\lambda = v/f$) and then calculate the limit of seperability (~$\lambda/4$) and visibility (~$\lambda/4$) (Brown, 2011). Our calculations indicate that the limit of seperability and visibility at the top of the studied section are ~17–21 m and 2–3 m respectively, and at the base of the studied section, these values increase to ~60 m and ~8 m (see Supplementay 2 for calculations). This resolution is sufficient to enable the investigation of small errors in our analyses caused by the three elements of interpretation uncertainty we are interested in.

3.2. *Geological setting*

The study area is situated in the Exmouth Plateau region of the Northern Carnarvon Basin, offshore NW Australia (Fig. 4a). The region

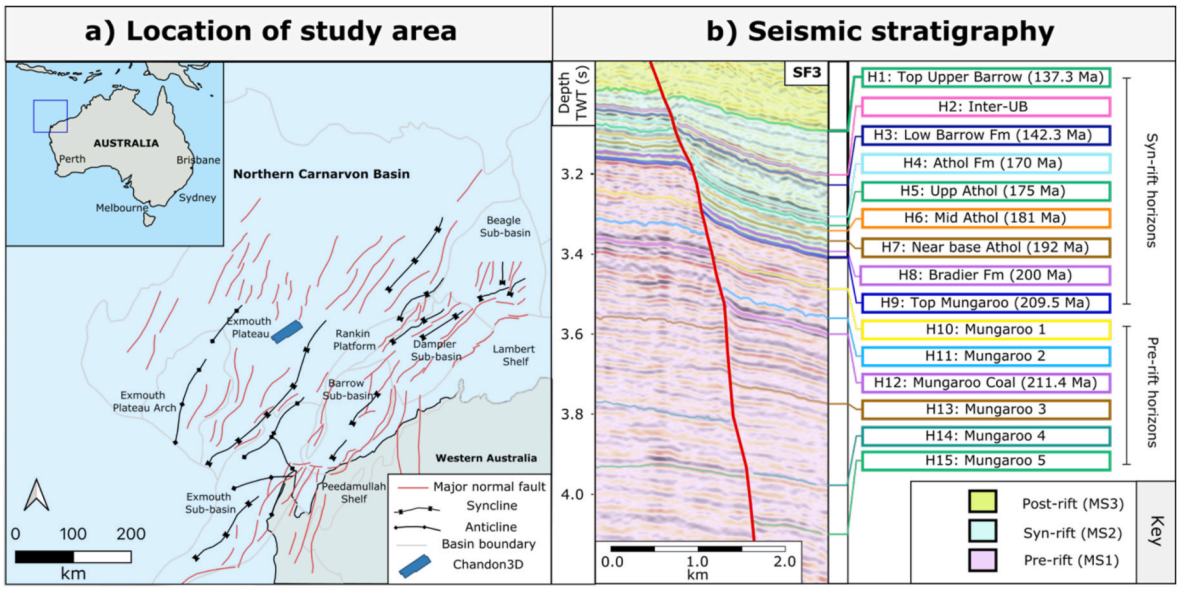

Fig. 4. Regional geology and seismic stratigraphy: a) a) Overview of the North Carnarvon Basin showing the major faults and sub-basins (adapted from Bilal and MacClay, 2021). The study area, as marked as a blue box, is not located on one of the major faults and as such displays little footwall degradation compared to other faults in the area; b) Seismic stratigraphy highlighting the key horizons used in this study. MS referes to the megasequences referred to in Bilal and McClay (2022). (For interpretation of the references to colour in this figure legend, the reader is referred to the Web version of this article.)

experienced several phases of rifting from the Late Carboniferous to the Early Cretaceous (Tindale et al., 1998; Stagg et al., 2004; Direen et al., 2008). The Triassic to recent tectono-stratigraphy of the Exmouth Plateau can be divided into four main megasequences (Fig. 4b) (Bilal and McClay, 2022). The main phase of WNW-directed extension, which is associated with deposition of Megasequence-II, resulted in the formation of north-south striking normal faults, including three of the four faults we focus on (SF1, 3, 4) (Fig. 5) (Stagg et al., 2004; Bilal et al., 2020; Bilal and McClay, 2022). During rifting, the basin was sediment-starved, meaning it now contains a relatively condensed ($\lesssim$100 m thick) of a largely marine syn-rift succession (Karner and Driscoll, 1999). This succession is separated from the overlying Late Jurassic marine Dingo Claystone by the end-Callovian regional unconformity (Tindale et al., 1998; Yang and Elders, 2016; Bilal et al., 2020; Bilal and McClay, 2022). Tectonic faulting slowed, or stopped, during the Late Jurassic, but resumed after formation of the regional unconformity (~148 Ma), being synchronous with the deposition of the Barrow Group (~148–138 Ma) (Gartrell et al., 2016; Reeve et al., 2016; Paumard et al., 2018). During the second phase of faulting, new N–S to NW-SW striking, low-throw (<0.1 km) normal faults developed (Black et al., 2017), with some of the earlier faults being reactivated (Bilal and McClay, 2022). Continental breakup occurred during the Early Cretaceous (~135–130 Ma) and was followed by thermal subsidence and passive margin development (Robb et al., 2005; Direen et al., 2008; Reeve et al., 2021).

In addition to tectonic faults, a series of dyke-induced faults are identified across the study area (Magee and Jackson, 2020a, 2020b; Magee et al., 2023), of which SF2 (Fig. 5b) is an example. These dykes are expressed as sub-vertical, low-amplitude zones that disrupt the seismic reflectors within the pre-rift sedimentary succession (Magee and Jackson, 2020b). Several associated grabens occur directly above and along the dykes, bound by oppositely dipping faults that intersect with the upper dyke-tip (Magee and Jackson, 2020a, 2020b). These dyke-induced faults are often long (10 s km), show variable dip and displacement distributions along strike, typically have low maximum throw values (often <50 m), and terminate upwards at the Base Cretaceous unconformity (Magee and Jackson, 2020a, 2020b; Magee et al., 2023).

Four sub-linear faults (SF1-4) were analysed in this study, varying in length from 2.4 to 7.9 km and exhibiting maximum total throw (i.e., throw extracted using continuous cut-offs) ranging from 32 to 273 m (Fig. 5f–i). Discontinuous and continuous cut-offs can be measured for faults SF2-4; however, the average throw across SF1 (13 ± 6 m) is between the limit of separability and visibility for the seismic cube. Therefore, only a small number of picks along this fault display discontinuous throw. We report only data extracted from continuous cut-offs for this fault. It is also expected that greater uncertainty will be observed for this fault due to the lack of discrete deformation to guide cut-off picking (Magee et al., 2023). Fig. 5f–i shows the throw distributions of the base syn-rift horizon (H9), showing variations between faults. Along Horizon 9, faults exhibit moderate dips (52° ± 8°) with lower dips observed at shallower depth, within the syn-rift succession (H1 = 32° ± 6°).

The studied faults have been buried beneath a thick layer of post-Cretaceous sediments, which can lead to compaction and rotation of pre-existing structures to shallower dips (Allen and Allen, 2013). Burial-related compaction will also act to reduce the throw across syn-sedimentary faults by <15% in sand-shale mixed lithologies (Taylor et al., 2008) similar to those observed in the study area (Bilal and McClay, 2022). However, decompaction was not performed in this study due to uncertainties in decompaction parameters, particularly for more deeply buried hanging wall sediments not sampled by well data. As a result, the extracted values of fault throw, dip and displacement represent minimum estimates. Since all faults have been buried to a similar depth, the impact of compaction on the extracted fault properties should be consistent across the datasets, and thus should not affect our statistical analysis or related conclusions.

3.3. Sample strategy

Oblique transects, relative to fault strike, were created close to the location of maximum fault throw for each fault. The transects were created at obliquity intervals of 10° from perpendicular (0°) to the faults at this point. This resulted in 11 transects, at different obliquities (i.e., from 0° to ±50; Fig. 1a) for each fault. Each transect was then transposed to parallel positions along each fault at a separation of 100 m (following the strategy shown in Fig. 1a). This means that for the oblique analysis, the along-strike distance between adjacent cut-offs is > 100 m

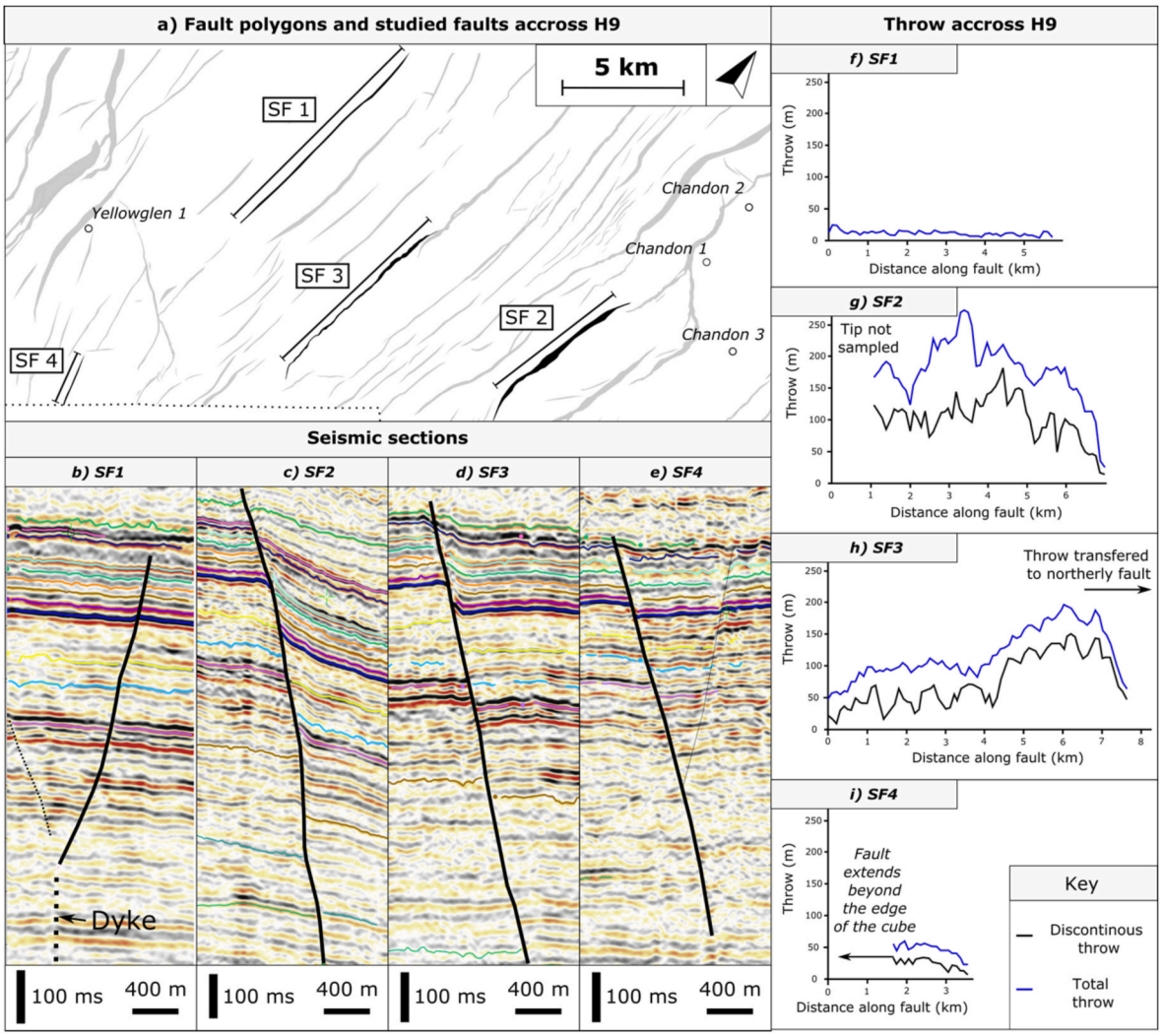

Fig. 5. Studied faults: a) fault polygons for Horizon H9, highlighting the location of the four quasi-straight faults studied; b-e) strike-perpendicular transects for each fault showing the structural style of each fault; f-i) along-strike profiles depicting the thow extracted using discontinuous (black) and continuous (i.e., total throw) (blue) cut-offs across the H9 horizon for data extracted using a strike-perpendicular transect. Note that the difference between the two lines represents the magnitude of deformation accommodated by folding and/or sub-seismic scale faulting. (For interpretation of the references to colour in this figure legend, the reader is referred to the Web version of this article.)

(~156 m for 50° obliquity) and the exact location on the fault the data is collected from differs between transects of different obliquity.

At each sample location (i.e., every transposed position where the fault is exposed along each transect for each angle of obliquity), we collected discontinuous and continuous cut-off data for 8–13 horizons, the actual number in each instance is determined by the regional continuity of mapped reflectors. For discontinuous cut-offs, we identified the location where the horizon intersects the fault in the footwall and hanging wall; for continuous deformation, we projected the regional horizon dip onto the fault plane (Fig. 1b). Depth values were converted from two-way travel time (TWT) to metres, and the following fault properties were calculated: throw, heave, dip, and displacement (Fig. 1a and b). For dip and displacement, we assumed that the slip vector is dip-parallel (cf. Magee and Jackson, 2020a). Where both discontinuous and continuous cut-offs are extracted (SF2-4), we also calculated the ratio between the different types of throw.

To test the repeatability of interpretation, and the impact on fault properties, picks of horizon H9 and H12 were repeated. These horizons were selected as their seismic reflection characteristics are similar, and because both horizons could be correlated across the study area. Fault interpretations were undertaken by a single interpreter (lead author Andrews) to ensure no inter-interpreter bias (e.g., Magee et al., 2023). There was a minimum period of three months between fault interpretations to reduce observations made during interpretation 1 directly effecting the 2nd interpretation. Andrews has 2–3 years experience of interpreting faults and picking fault cut-offs; familierisation with the seismic cube increased during the study, with continued interpretation. Whilst experience has been shown to effect seismic interpretation (Bond et al., 2007; Bond 2015); other studies (e.g., Magee et al., 2023) show that interpretation by the same individual, resulted in fault data of a similar magnitude to that derived from interpretations of the same dataset, completed by interpreters with a range in experience of up to >10 years.

To facilitate the plotting and comparison of data between oblique and strike-perpendicular transects, we determine the equivalent sample location of the cut-offs relative to the strike-perpendicular transect. For oblique cut-offs, the equivalent strike-perpendicular sample location will differ for the footwall and hanging wall (Fig. 1a). To account for this, we take an average of the two cut-offs to obtain the equivalent strike-perpendicular sample location on the fault.

3.4. Data presentation and statistical analysis

We analyse and present our data on discontinuous vs continuous fault cut-off choice, transect obliquity and interpretation repeatability, using statistics derived from the whole dataset statistics and by comparing individual picks at a given location along the fault. Dataset statistics involve statistically comparing population means or medians to determine ther equivalence, with our approach outlined in Supplementary 7. To compare datasets based for a specific uncertainty element (e.g., obliquity, cut-off type), we report the average difference between population means, the average percentage (%) difference, and the proportion of datasets that can be considered equivalent. Aggregated dataset statistics allow for a direct comparison of properties across faults that have different lenths, and therefore a different number of cut-off picks. Initially, we combine and discuss the obliquity and repeatability statistics for each fault property (i.e., take the average values for absolute difference, % difference, and % of equal datasets of the discontinuous and continuous datasets). Subsequently, we compare discontinuous and continuous fault cut-off data, transect obliquity and interpretation repeatability datasets in the same manner (see Supplementary 7, for the full analysis).

4. Results and the impact of uncertainties on fault properties

We initially discuss the effect of our three investigated uncertainty elements (discontinuous and continuous fault cut-offs, transect obliquity and interpretation repeatability) for datasets containing data from all extracted fault properties (Section 4.1), before considering their impact on individual properties (i.e., throw, heave, displacement, dip) (Sections 4.2 to 4.4).

4.1. All fault properties

Repeatability: Of the repeatability datasets, only 46% (283 out of 616) were statistically equivalent, with an average difference in population mean/median of 16% (Table S1). The percentage of equivalent datasets varied between faults, ranging from 31% (SF1) to 56% (SF2), and the difference in population means ranged from 9% (SF2) to 28% (SF1). Repeat picks showed more uncertainty for horizon H9 (32% equivalent datasets, 20% difference) compared to H12 (59% equivalent datasets, 13% difference). This trend was consistent across all faults, although the magnitude of difference varied between faults. Overall, less than half of the repeat horizons could be considered equivalent.

Obliquity: Greater errors were observed where the degrees of obliquity exceeded 20° (Fig. 6). The same overall pattern was observed for individual faults, although there was more scatter in the data (Fig. 6). The percentage difference for any given obliquity also varied for each fault. Some horizons are more prone to obliquity related errors (Table S2), suggesting that horizon properties contribute to interpretation errors. For example, H9 which has stronger reflectivity (Fig. 2a) displays lower percentage differences when compared to H1, where reflectivity is weaker (Fig. 2a–Table S2). Nevertheless, all horizons exhibited the same general trend of increased uncertainty with increasing obliquity.

Interpreted cut-off type: The effect of cut-off type differed between obliquity and repeatability datasets. For repeat interpretations, little difference was observed in the uncertainty between continuous and discontinuous cut-offs, with 48% and 44% of datasets considered equal. Conversley, the obliquity datasets displayed greater uncertainty for continuous cut-offs (51% equal datasets) when compared to discontinuous cut-offs (63% equal datasets) (Table S2). Certain horizons showed greater uncertainty in data extracted from continuous cut-offs (e.g., H13 and H14); however, this was not always the case with uncertinaty being high (e.g., H1, H3, H11) or low (e.g., H9, H13) for both cut-off types for a given horizon (Table S2). This suggests the interpreted cut-off type has a moderate effect on obliquity datasets and a minor to negligible effect on repeat picks, with the horizon from which the data is extracted being a key controlling factor on the magnitude of uncertainty.

Overall, when considering all fault properties: the interpreted cut-off type, the magnitude of obliquity, and the fault and horizon from which the data is extracted, are identified as key factors controlling interpretational uncertainty. To assess the effect of obliquity on repeatability, it is important to separately considered the influence of uncertainty factors on each fault property separately. This approach allows for the isolation of factors and the comparison of obliquity errors to the theoretical errors introduced in Fig. 3.

4.2. Throw

Repeatability: Throw exhibits low uncertainty across all repeatability datasets (Table S1, Figs. 7 and 8), with 60% of datasets considered equivalent, and there being only small differences in means (5 m, 7.4%). The mean absolute difference differs between faults, with differences across all faults typically below the estimated seperability limit of the seismic data (Table S1). Whereas differences in population means are minimal, this was not the case for all picks along the fault. For example, Fig. 9a and c shows multiple locations where the difference between picks on throw profiles extracted from discontinuous and continuous cut-offs exceeds 22 m. The profiles also highlight sections of the fault with high and low differences between picks, and that the location of

Obliquity	a) % of oblique datasets that are statistically equal to the fault perpendicular dataset					Colour scale	b) % error between oblique and fault perpendicular datasets					Colour scale
	SF1	SF2	SF3	SF4	All faults		SF1	SF2	SF3	SF4	All faults	
-50	20%	28%	29%	54%	34%	Maximum value	65%	28%	38%	35%	38%	Minimum value
-40	45%	19%	38%	64%	40%		26%	26%	26%	22%	25%	
-30	61%	38%	45%	83%	54%		17%	15%	17%	15%	16%	
-20	73%	72%	74%	88%	77%		13%	10%	8%	12%	10%	
-10	80%	84%	91%	95%	89%		16%	6%	4%	9%	7%	
10	73%	58%	66%	86%	70%	Median	13%	10%	10%	11%	11%	Median
20	61%	88%	56%	85%	73%		19%	6%	12%	14%	12%	
30	39%	38%	42%	88%	52%		5%	15%	16%	18%	19%	
40	57%	30%	31%	58%	41%		21%	22%	25%	29%	25%	
50	30%	23%	22%	64%	34%	Minimum value	43%	41%	42%	25%	38%	Maximum value
Total	**54%**	**48%**	**49%**	**76%**	**56%**		**27%**	**18%**	**20%**	**19%**	**20%**	

Fig. 6. The effect of obliquity on extracted fault properties: a) the % of datasets for that fault and obliquity that are statistically equal to the dataset extracted for that horizon using a strike-perpendicular transect; b) the percentage error of all fault properties split by fault and obliquity. Colour scales differ between individual faults and all fault datasets so that red represents datasets that are highly affected by obliquity, and blue represents datasets where obliquity has a limited effect on extracted fault properties. Note how most values are blue (smaller errors) where obliquity is $<\pm$ 20°, suggesting that oblique sampling above this value should be avoided to minimise obliquity related errors. (For interpretation of the references to colour in this figure legend, the reader is referred to the Web version of this article.)

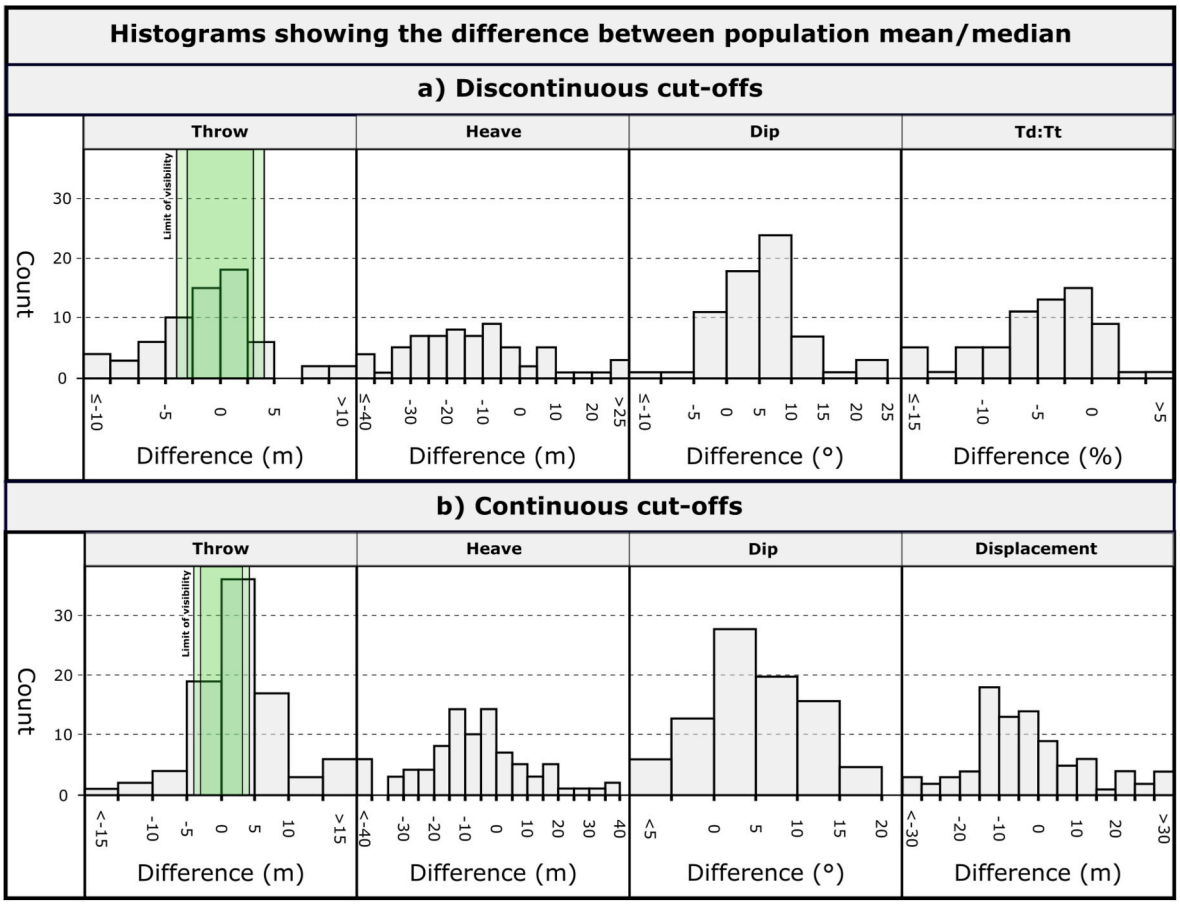

Fig. 7. Histograms to summarise the mean/median difference in fault properties extracted from discontinuous (a) and continuous (b) cut-offs between repeat picks at identical points, across a series of horizons and faults. Each 'count' represents a population mean or median for all data points collected for a single horizon across a single fault. The green box on the throw histograms highlights the minimum and maximum limit of visibility for the seismic cube. Differences within this box can be considered as below the resolution limit, and therefore not caused by repeatability errors. Note that for all extracted properties, continuous measurements show lower repeatability than discontinuous measurements. (For interpretation of the references to colour in this figure legend, the reader is referred to the Web version of this article.)

these sections are not consistent between horizons (i.e., H9 may show high variability at a particular along-strike location where H12 shows low variability, and vice versa). This suggests that whereas horizons have a limited effect on population statistics, they do influence individual picks. Overall, repeatability errors primarily affect throw at a local scale (e.g., <500 m along strike distance) and have a negligible effect on population statistics.

Obliquity: Overall, throw typically displays increasing uncertainty as the obliquity increases (Table S2, Fig. 10); however, the error across the range of obliquity is low. Where individual faults are considered, not all faults show greatest error at high degrees of obliquity (e.g., SF1, SF4; Table S3). The picked horizon also has a large impact on the % difference for throw, although the overall trends of increasing uncertainty with increasing angles of obliquity are still observed. The distribution of throw across the fault plane varies at different degrees of obliquity (Figs. 11, 12a and 12e) and can be over- or under-estimated at different locations, with % errors locally exceeding 100%. We suggest that changes in imaged horizon properties (e.g., acoustic impedence, amplitude of the reflection) influence the picked cut-off data and hence throw measurements. Obliquity errors exceed the theoretical geometrical errors (Fig. 3) for throw for faults by <±5%, with some horizons exceeding the expected error by a factor of 5 (Fig. 10). The repeatability of throw does not appear to be sensitive to the degrees of obliquity as highlighted by: i) the distribution of statistically equal datasets and ii) given angle of obliquity can show both high and low % differences for the same cut-off type and horizon (Fig. 13).

Interpreted cut-off type: The interpreted cut-off type affects the magnitude of repeatability and obliquity errors. Average repeatability errors for throw are marginally higher for continuous cut-offs (6.0 m, 9%) compared to discontinuous cut-offs (4.0 m, 5%) (Table S1). In most cases, H9 showed greater errors compared to H12 for both cut-off types, with the only exception being continuous cut-offs extracted from SF2 (Table S1). The magnitude and location of along-strike variations between individual picks differed between horizons and cut-off type (Fig. 9). Indeed, there are examples where throw calculated from the first discontinuous cut-off pick exceeds the second, with the opposite being true for continuous cut-offs. For oblique transects, a far greater proportion of datasets are equal (91%), with a lower % error (7%) for discontinuous cut-offs when compared to continuous cut-offs (75%, 11%; Tables S7 and S8). The magnitude of error increases for low-throw faults where the same horizons show large and small error, albeit with continuous cut-offs showing greater errors. The distribution of throw along- and down-dip is highly variable at different degrees of obliquity (Figs. 11, 12a and 12e), with the distribution and magnitude of throw depending on the direction and degree of obliquity. Additionally, the patterns are not constant between discontinuous and continuous cut-offs, as shown by the location of throw maxima in Figs. 11 and 12a, e.

4.3. Heave

Repeatability: Heave shows high uncertainty across all repeat picks (Figs. 7 and 8), with only 37% of datasets considered equivalent and a

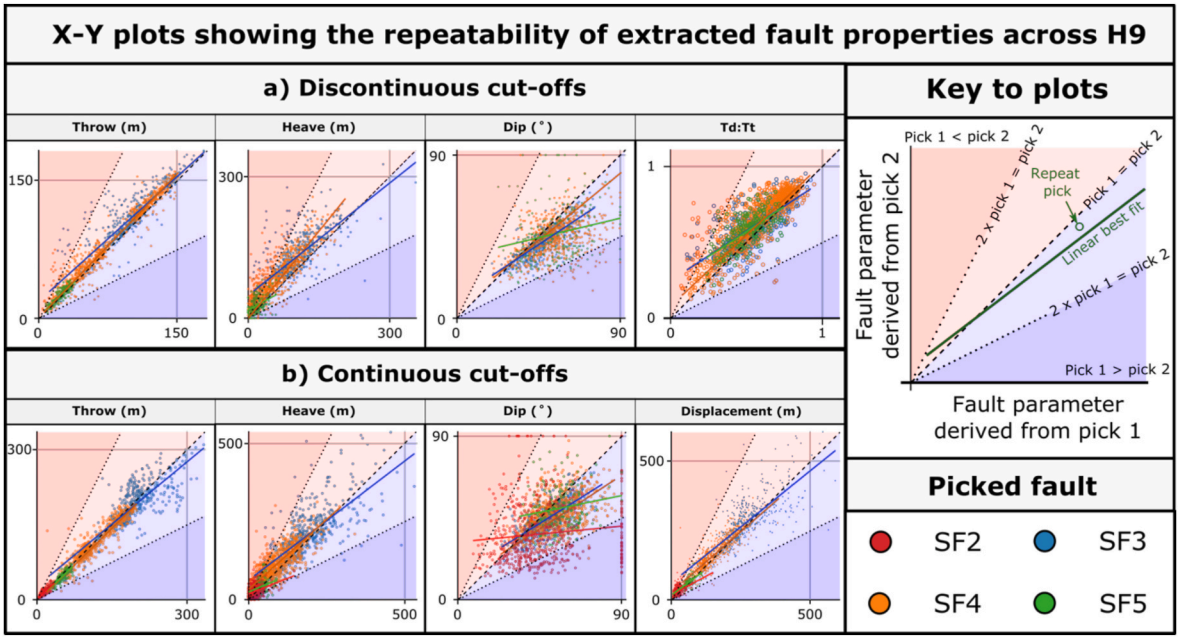

Fig. 8. x-y plots showing the variations in repeatability in discontinuous (a) and continuous (b) fault properties extracted from horizon H9 across all faults. If the interpretation is repeatable, then all points should plot along the black dashed x-y line; however, where picks differ the points will plot within the red or blue zone depending on the ratio of pick values. Data plotting in the darker red or blue zones represent data where one pick is over double the other. Note how the difference between picks varies between faults, extracted property, and the magnitude of the extracted property. Additionally, throw shows less repeatability error than heave. (For interpretation of the references to colour in this figure legend, the reader is referred to the Web version of this article.)

reasonable difference between population mean/median values (17.8 m, 27%). SF2 is less prone to repeatability errors when compared to other faults (Fig. 8; Table S1). Repeatability errors are greater at lower values of heave, as indicated by the higher % difference for SF1 and the x-y plots in Fig. 8. Along-fault heave profiles (Fig. 9b–d) show a large variability in the magnitude and difference between picks for adjacent measurement positions (i.e., a large amount of noise in the data). Errors are not consistent between horizons or measurement types and the difference between picks locally exceeds 50 m (Fig. 9b–d). This suggests that repeatability errors in fault and horizon picks and how these vary along-strike effect the extraction of heave, creating uncertainty in heave measurements.

Obliquity: The degree of obliquity has a large effect on heave, with uncertainty increasing with increasing degrees of obliquity (Table S4). The mean absolute difference in heave exceeds the average difference for repeat picks at obliquities of ±30° and shows a maximum difference of 54.3 m (72%). This trend is observed across all faults; however, each fault shows a different magnitude of error and proportion of equal datasets, with SF2 and SF3 appearing to be most prone to obliquity errors. When compared to theoretical geometric errors (Figs. 3 and 10) most datasets show % errors that exceed the expected values by between 5% and 10%, with the heave measurement for some horizons being particularly prone to high errors. The effect of obliquity on the distribution of heave across the fault plane depends on the fault and the direction and degree of obliquity (Fig. 12b–f). For all faults, the overall trend is that as obliquity increases, the proportion of positive % difference also increases (irrespective of the absolute magnitude of heave). On top of these general trends however there is a large amount of scatter in the data, which for some faults (e.g., SF1) lead to a high spatial variability in heave (Fig. 12b–f). For all datasets, the angle and direction of obliquity does not appear to affect the % difference between picks (Fig. 13). Overall, the degree of obliquity greatly affects the measurement of heave, with the error compounded by large differences between along-strike sample locations.

Interpreted cut-off type: The interpreted cut-off type has a large effect on obliquity statistics, although the effect on repeatability depends on the fault which the data are extracted from (Table S1, Fig. 13). For repeat picks, heave extracted from continuous cut-offs shows a smaller difference in population mean (16.5 m, 26%) and a higher proportion of equivalent datasets (41%) compared to discontinuous cut-offs (19.0 m, 33% and 28% respectively). However, this is not the case for SF2 where the opposite is true. Both cut-off types show large along-strike variability; however, continuous cut-offs show less difference between adjacent sample locations than discontinuous cut-offs (Fig. 6). The measurement of continuous cut-offs greatly increase the % error in obliquity statistics, with the error nearly always greater than discontinuous cut-off data and the theoretical geometrical error (Figs. 1c and 7). Smoother profiles observed in the repeatability datasets are mirrored where heave is calculated from continuous cut-offs, with these strike projections appearing less noisy than the discontinuous cut-offs (Fig. 12b–f).

4.4. Displacement

Repeatability: Displacement shows moderate uncertainty across all repeat picks (Table S1, Figs. 7 and 8) with 47% of datasets considered equivalent and an absolute difference of 15.3 m (16%). The level of uncertainty differed between faults, with SF1 displaying the lowest number of equivalent datasets (27%) and greatest % error (31%). The along-strike displacement profiles (Fig. 9e) show the same along-strike variability observed in the heave profile, but with a lower magnitude of variability caused by the low variation in throw. Sections of faults that show high, or low, differences between picks are more laterally extensive (up to 1.5 km) than heave and match more closely the differences observed in throw (Fig. 9e).

Obliquity: Displacement exhibits increasing uncertainty at higher degrees of obliquity, surpassing repeatability errors at ±30° (Table S5). The pattern observed in heave strongly impacts the population statistics, with SF2 and SF3 showing the lowest proportion of consistent datasets. Displacement varies across fault planes, with increasing magnitude at higher obliquities (Figs. 10 and 12c, g). Like the heave datasets, the base syn-rift (H9) displays a pronounced displacement maxima and

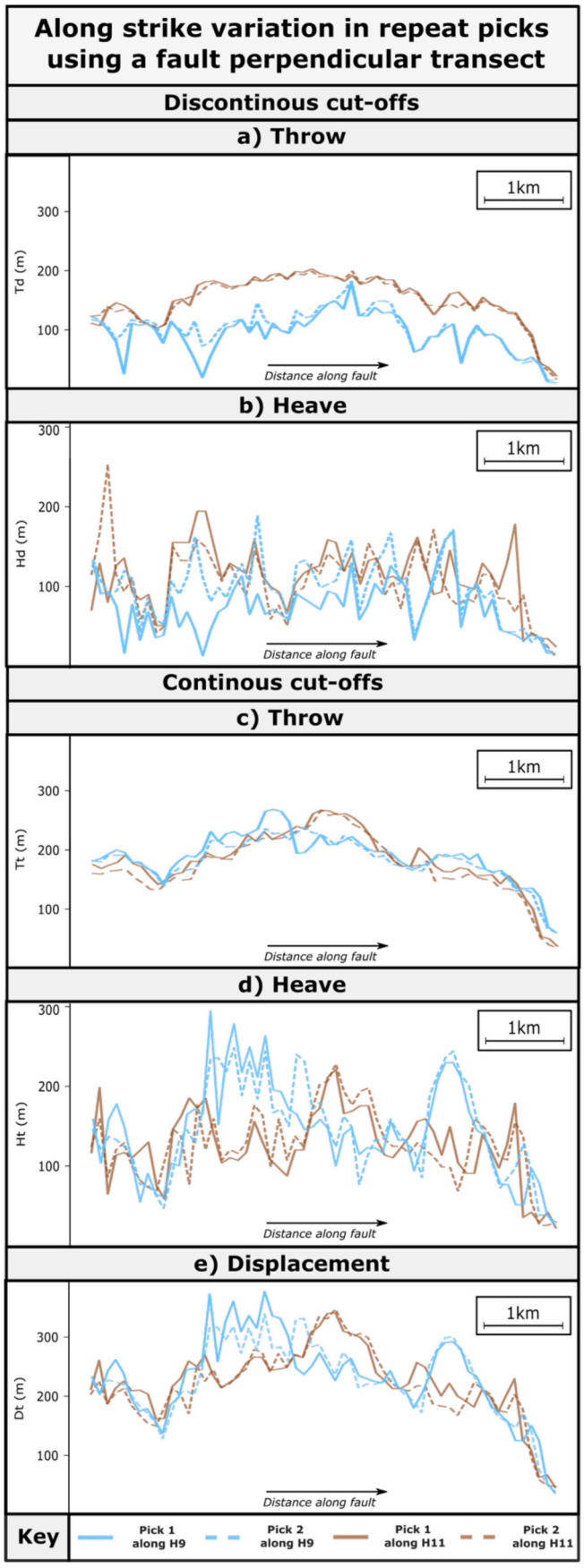

(caption on next column)

Fig. 9. Along-strike profiles showing the repeatability of fault property extracted from H9 and H12 using a strike-perpendicular transect along SF2. Pick one is shown as a solid line, whilst pick two is dashed and each horizon is a different colour. Note how the general shape of the profiles are similar between picks; however, the difference can be locally quite large. (For interpretation of the references to colour in this figure legend, the reader is referred to the Web version of this article.)

significant variability between along-strike data points (Fig. 12c–g). Measurement obliquity does not systematically effect the repeatability of fault displacement (Fig. 13). Overall, displacement is more susceptible to degree of obliquity than throw, with uncertainty in heave influencing the magnitude of displacement and how this varies along the length of the fault.

Interpreted cut-off type: Interpreted cut-off type impacts repeatability and obliquity errors differently (Table S1, Figs. 8 and 10). Displacement calculated from discontinuous cut-offs exhibits greater differences between picks, and a lower proportion of equivalent datasets compared to continuous cut-offs (Table S1). Both cut-off types show increasing uncertainty with increasing degrees of obliquity; however, the magnitude of difference is greatest for continuous cut-offs (Fig. 10). However, for some faults, highly oblique continuous cut-off datasets may exhibit low uncertainty (e.g., SF4, Table S12) and the displacement strike projections constructed for continuous cut-offs are smoother than discontinuous cut-offs (Fig. 12c–g). Despite this, repeatability errors are usually exceeded where measurement obliquity is at or above ±30°. Overall, interpreting continuous cut-offs reduces the repeatability of displacement on some horizons and measurement obliquity greatly affects continuous datasets.

4.5. Dip

Repeatability: Of all the fault properties, dip exhibits the highest uncertainty in repeat picks (Figs. 7 and 8, Table S1), with only 32% of datasets considered equivalent and an absolute difference of 6.6° (16%). The fault from which the data is extracted influences the magnitude of uncertainty in dip, with SF1 showing a mean absolute difference of 9.2°, whereas SF2 only has a difference of 3.2°. Unlike heave and displacement, the magnitude of dip appears to only have a weak effect on repeatability (Fig. 8). Individual picks on SF1 show very large differences, with several picks having a dip of 90° (indicating zero heave), whereas the paired pick ranges from ~15° to ~65° (Fig. 8). These picks are taken from where there are very small offsets along SF1, thus heave is likely below the resolution of the data here (minimum heave values of ~6 m). Due to the compound errors caused by the uncertainty in heave, dip shows low repeatability and along-strike variations can be masked by measurement errors.

Obliquity: Fault dip is strongly affected by measurement obliquity, with repeatability errors exceeded for most oblique datasets (Fig. 10, Tables S1 and S5). In a similar manner to displacement, the effect of uncertainties on heave strongly affects the calculation of dip (i.e., SF2 and SF3 showing the lowest % of equal datasets), although greater uncertainty is observed for the latter (Table S5). Repeatability errors are exceeded where the angle of obliquity exceeds ±20° for all faults, apart from SF1 where repeatability errors were particularly high (Table S5). The distribution of dip across the fault plane displays a high degree of variability between points leading to noisy strike-projections (Fig. 12d–h). Despite this, general trends are observed across all obliquities (e.g., shallower dips at the syn-rift horizon (H9)); however, the magnitude of dip is lower at higher degrees of obliquity. In most cases, there is no correlation between the degree of obliquity and repeatability (Fig. 13).

Interpreted cut-off type: The choice of cut-off type affects repeatability and obliquity datasets differently. Across all faults, the choice of cut-off type does not affect the repeatability of dip, with similar differences and percentage of equal datasets observed. Whether discontinuous or

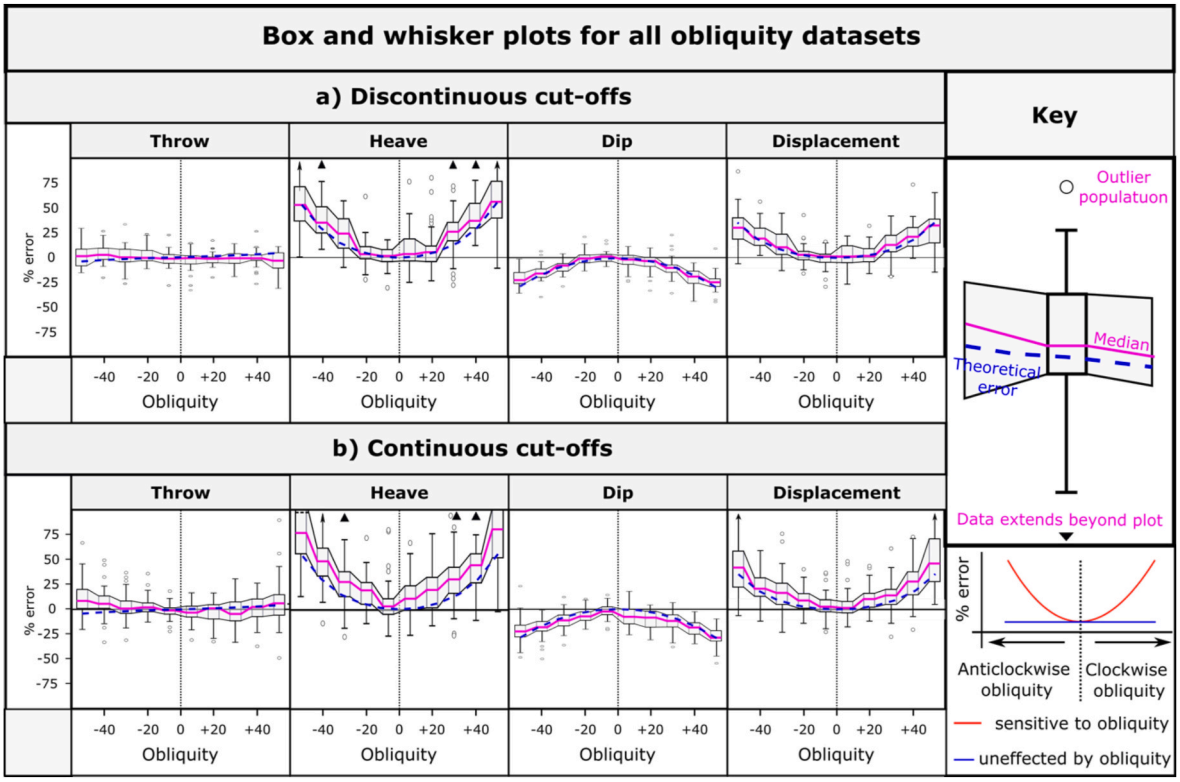

Fig. 10. The effect of obliquity on individual fault properties extracted from discontinuous (a) and continuous (b) cut-offs. Box and whisker plots are constructed from the population mean/medians of individual horizons picked across individual faults. Note how obliquity has the greatest effect on heave, and therefore dip and displacement, suggesting that additional care needs to be taken when sampling fault cut-offs for these properties. Furthermore, the median % error for all datasets typically exceeds the theoretical value for continuous cut-offs, suggesting some of the error is caused by non-geometrical effects.

continuous cut-offs, uncertainty depends on the fault and horizon the data is collected from, with H9 broadly showing greater uncertainty than H12 (ref a figure or table). When individual cut-off picks are considered, there is more scatter in the continuous cut-off data, than the discontinuous, (Fig. 8), with many picks exceeding 100% difference. Despite this, profiles constructed from continuous cut-offs show less along-strike variability (Fig. 9). Measurement obliquity affects both cut-off types; however, the effect is greater for continuous cut-offs (Tables S13 and S14). This trend is observed across all faults, however, the magnitude of error and difference between cut-off types depends on the fault and the horizon that the data are extracted from. It is difficult to assess the effect of cut-off type on the distribution of dip across the fault plane as both exhibit a highly variable distribution of dip for all datasets (Fig. 12d–h). Overall, no systematic difference between cut-off type is observed for dip repeatability, and whereas the measurement of continuous cut-offs increases errors associated with obliquity, datasets are very noisy and it is not possible to deduce along-fault trends.

4.6. Summary of results

Our data show that fault properties extracted from fault-horizon cut-offs are variably influenced by interpretation repeatability, measurement obliquity, and the measured cut-off type (Table 1). When all properties were considered together, less than half of the datasets could be considered statistically equal. Errors due to measurement obliquity were found to greatly increase when obliquity exceeded ±20°. Measurements of continuous cut-offs showed greater errors than discontinuous cut-offs in both the obliquity and repeatability datasets. The magnitude of error was also influenced by which fault and horizon the data were collected from.

When individual fault properties are considered, throw is found to be the least sensitive fault property to the studied interpretation factors, and heave the most sensitive (Table 1). Uncertainties in throw increased when measurement obliquity exceeded ±20°; however, the magnitude of uncertainty was often below or close to the limit of separability of the seismic cube (i.e., not a significant source of error) apart from at a local (<500 m) scale. Heave was found to show statistically significant differences for both repeat and oblique datasets. Differences were particularly evident at a local scale and caused strike projections and along-strike profiles to be noisy. The fault and horizon cut-off that the data were extracted from had a subsidiary effect on extracted fault properties (e.g., heave and throw), with the magnitude of obliquity not compounding repeatability errors. Across most fault properties, continuous cut-off picks were more susceptible to repeatability and obliquity errors. Despite showing greater uncertainty for continuous picks, continuous datasets show less along-strike variability between adjacent picks, leading to smoother along-fault profiles and strike projections. The ratio of throw extracted from discontinuous to continuous cut-offs indicates that the errors from the continuous and discontinuous datasets were compounded where the properties were compared, and the noisiness of the discontinuous profiles lead to large variations in the ratio between discontinuous and continuous throw between adjacent picks across a fault. Uncertainty in heave also increases uncertainty in displacement and dip (as these properties are geometrically derived using heave), with the effect particularly noticeable in along-fault profiles and strike projections. For dip, it was found that this local scale uncertainty often masked overall trends in dip and caused profiles and strike projections to be very noisy (Fig. 12d–h).

In the following section, we investigate how our results on uncertainties in cut-off derived fault properties affect the assessment of fault transmissivity and the evolution of throw- and slip-rate through time. We make this investigation to demonstrate the potential impact of interpretation choices and repeatability on fault properties used in the

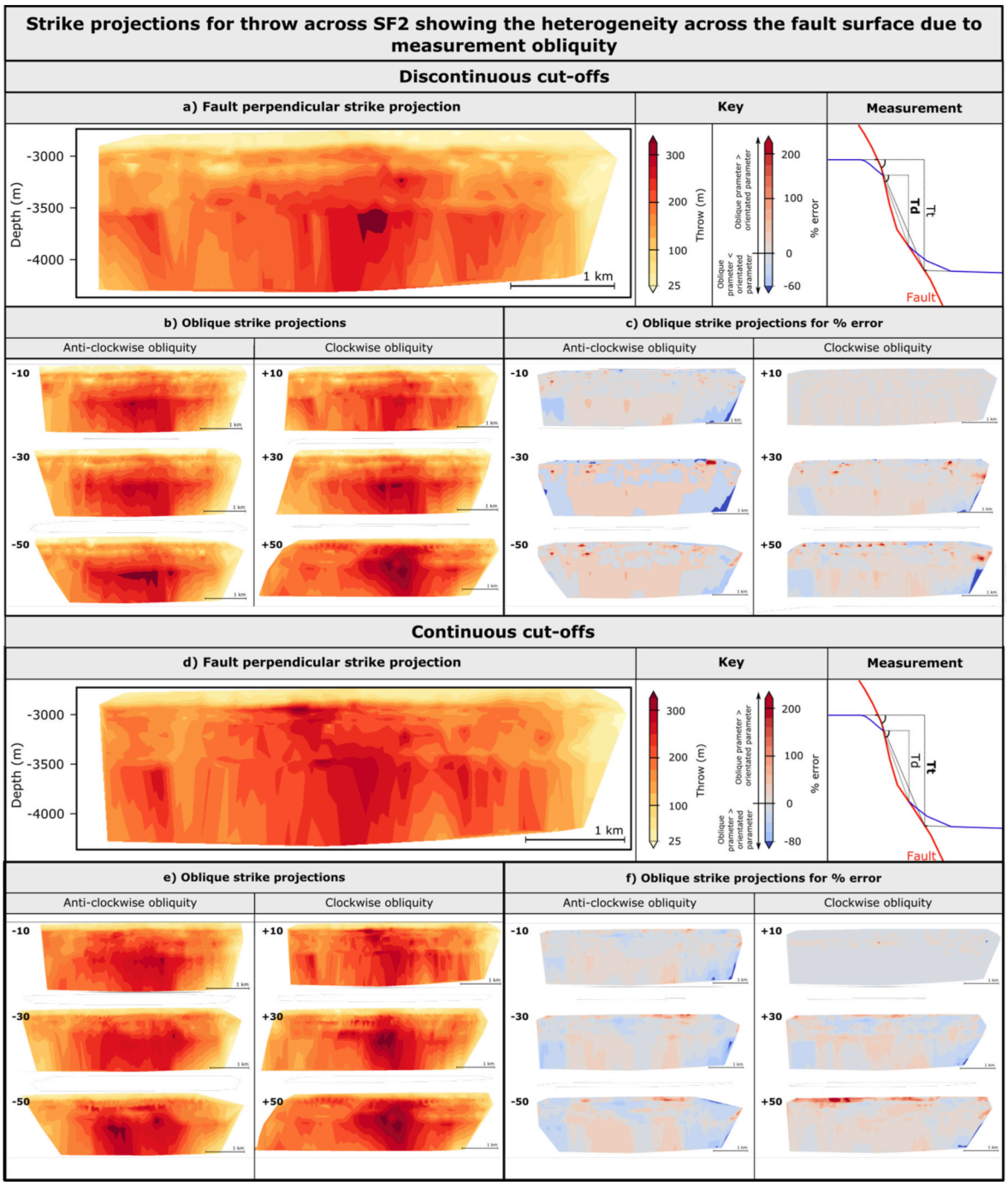

Fig. 11. Strike projections showing the along-strike and down-dip variability caused by oblique sampling for throw extracted using discontinuous (a–c) and continuous (d–f) cut-offs along SF2. Data extracted from strike-perpendicular (a & d) and oblique (b & e) transects are shown, along with the % error associated with the oblique measurement (c & f). Note how the distribution and % error of throw depends on both the direction and magnitude of measurement obliquity. Strike projections are created using a python script that undertakes a linear interpretation between known datapoints, resampled to a regular sample spacing to enable the % difference between datasets to be calculated.

prediction of crustal fluid-flow and in the assessment of seismic hazards.

5. Effect of obliquity and repeatability uncertainty on inferred fault properties

Data extracted from 3D seismic reflection surveys are used across a range of scientific studies, and therefore the sources of uncertainty presented in this paper have implications for the geological analyses that arise. Drawing on data from the interpretation of SF2, we discuss the implications for two such analyses, fault transmissivity which is important for quantifying fluid flow, and slip/throw rates used to inform seismic hazard assessment. Throw extracted from discontinuous cut-offs is used for fault transmissivity and throw-rate calculations, whereas continuous cut-offs are used when assessing the evolution of slip-rate to account for non-discrete deformation (e.g., monocline development). These examples demonstrate the practical effect of the investigated uncertainty elements on fault property predictions.

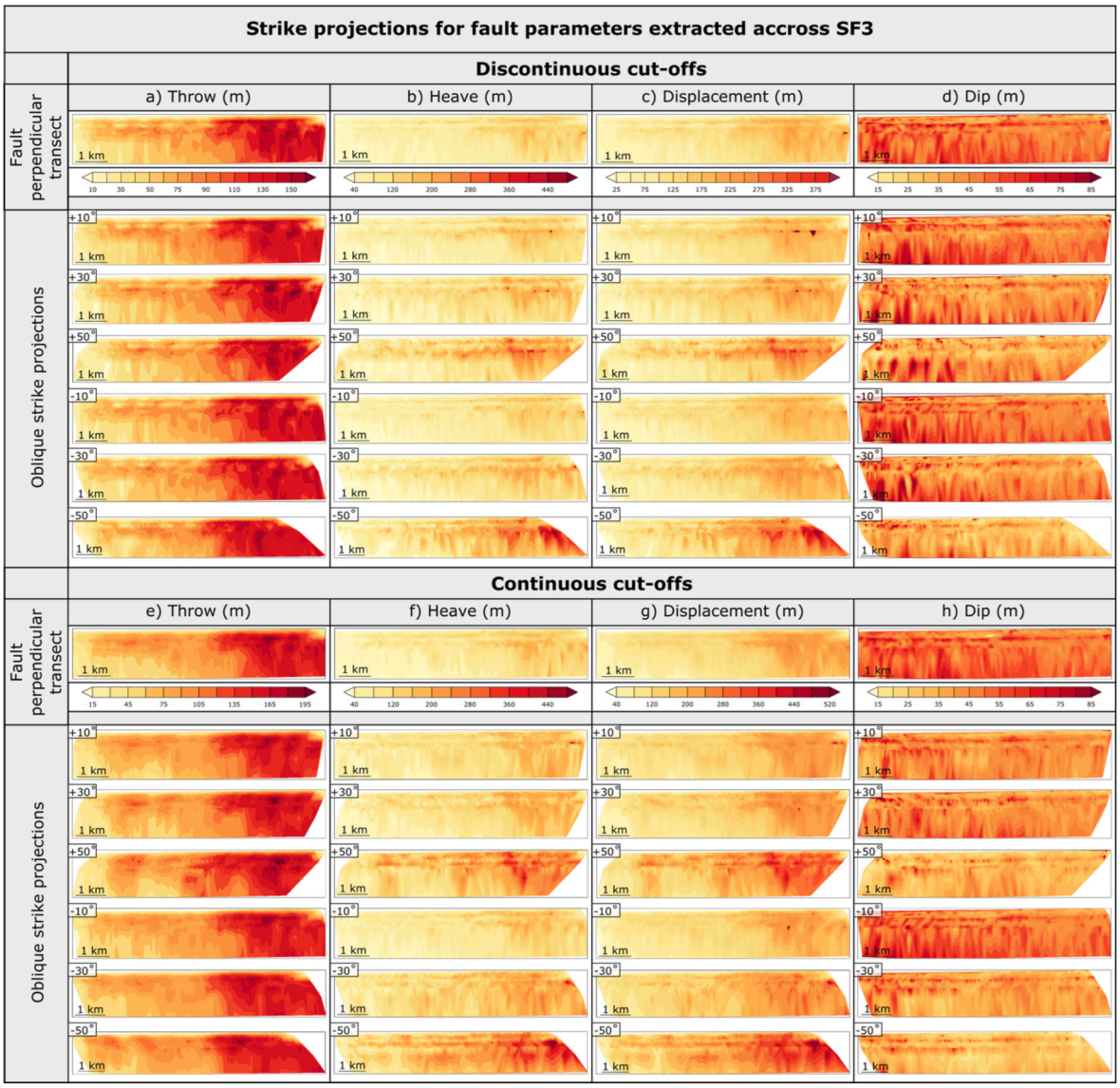

Fig. 12. Strike projections showing the along strike and down dip variably of all studied fault properties calculated from discontinuous (a–d) and continuous (e–h) cut-off data extracted from SF3. Note how throw is less sensitive to measurement obliquity than heave and displacement and that dip shows high spatial variability across all datasets.

5.1. Fault transmissivity interpretation using discontinuous deformation

Cross-fault transmissivity describes the ability of fluid to flow across a fault zone. The potential for cross-fault flow is important to quantify for hydrocarbon production, CO_2 sequestration and the geological disposal of nuclear waste. A common method used to assess fault transmissivity is to calculate the shale gouge ratio (SGR, e.g., Yielding et al., 2002), by considering the proportion of shale that has moved past a given point on a fault using the following equations:

$$V_{shale} = \frac{GR_z - GR_{min}}{GR_{max} - GR_{min}}$$

$$SGR = \frac{\sum (V_{shale} \times \Delta z)}{throw}$$

$$(\Delta z = bed\ thickness)$$

A higher SGR ratio suggests that there is a high proportion of phyllosilicates (shale) within the fault core (e.g., Foxford et al., 1998; Yielding, 2002). An SGR of 15–20% has been suggested as a sealing limit (Yielding, 2002); however, it should be noted that this value is based on relatively shallow resevoirs (<3 km) and that fault permeability may be

$$(V_{shale} = proportion\ of\ shale\ in\ a\ given\ rock\ volume, GR_z = Gamma\ ray\ reading\ at\ a\ specific\ depth, GR_{min} = minimum\ gamma\ ray\ reading, GR_{max} = maximum\ gamma\ ray\ reading)$$

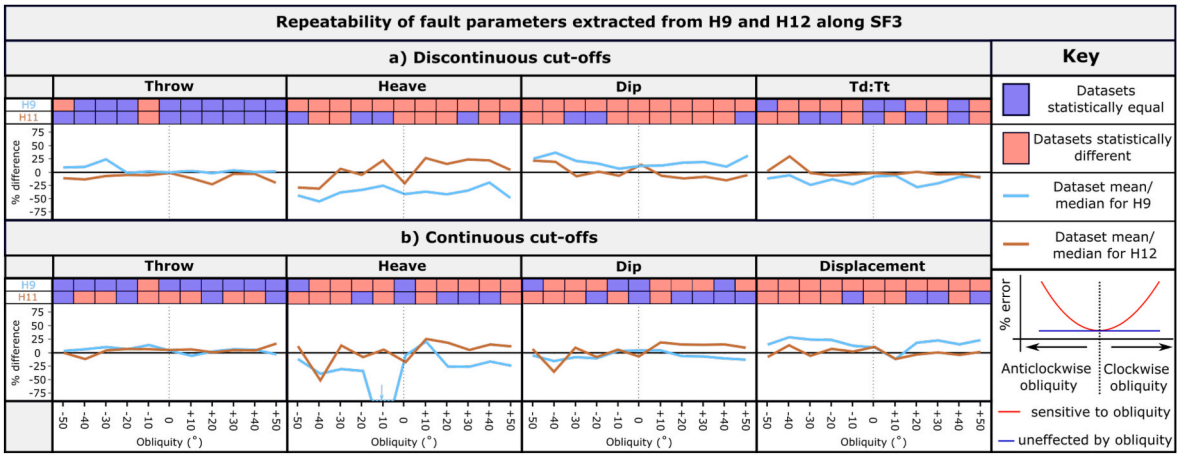

Fig. 13. Repeatability of fault picks for fault parameters extracted using discontinuous (a) and continuous (b) cut-offs along horizons H9 and H12 for SF3. The plots show whether pick one and pick two can be considered equal, and the mean % difference between each pick. Note how there is no correlation between obliquity and repeatability error, suggesting that obliquity and repeatability are independent sources of error for this dataset.

Table 1
Summary of the effects of interpretation uncertainty on the extracted fault properties. Note how heave is more prone to interpretational uncertainty than throw, which also affects the extracted dip and displacement.

Fault property	Repeatability	Measurement obliquity	Interpreted cut-off type
All fault properties	Repeat datasets are often not equivalent, with the % difference depending on the fault and horizon that the data is extracted from.	Error is found to increase where obliquity exceeds ±20°. The fault and horizon that the data is collected from also has a subsidiary effect.	Greater uncertainty in continuous cut-offs compared to discontinuous; however, the difference is low to moderate for obliquity datasets and negligible for repeat picks.
Throw	High repeatability Errors only significant at a local scale (i.e., <500 m).	Moderate sensitivity Errors increase as obliquity increases and are larger than predicted. Overall differences in population means are generally small.	High sensitivity Uncertainty increases in faults with low throw. Throw distribution is variable and influenced by the horizon and measurement obliquity.
Heave	Low repeatability Depends on the fault, horizon, and along-strike position that the data is collected form.	High sensitivity Errors are compounded due to differences between along-strike sample locations.	High sensitivity Continuous cut-off data exhibits smoother along-strike profiles but with increased errors at high obliquities.
Displacement	Moderate repeatability Along-strike patches of low repeatability more closely match the shape of the throw profile.	High sensitivity Due to high uncertainty in heave influencing the distribution and magnitude of displacement.	Moderate sensitivity Measurement obliquity greatly effects continuous cut-off datasets, whilst also causing strike projections to be smooth.
Dip	Low repeatability Along-strike variations are often obscured by measurement errors	High sensitivity Overall dip increases with obliquity, and there are large spatial variations across the fault plane.	Low sensitivity Datasets are very noisy and it is not possible to deduce along-fault trends.

orders of magnitude lower or higher than resevoir properties (Bense et al., 2013). In this section we investigate how the calculation of SGR is effected by differences in fault throw caused by measurement obliquity and repeatbality errors. Some software also enable fault displacement to be used as an input. Whilst we do not explore how displacement influences SGR in this section, the greater uncertainty caused by measurement obliquity, and lower repeatability, of displacement suggests that greater uncertainty in SGR will arise when displacement is used as an input. It should be noted that it is not our aim to characterise the sealing potential of SF2, but instead highlight how our findings may effect the calculation of SGR.

We manually calculate the SGR at each horizon-fault cut-off pair for the repeatability datasets of throw across SF2. Due to the large number of horizons and datasets, we assess how the differences in mean throw effect SGR for each horizon and degree of obliquity. The purpose of using mean values is to demonstrate the impact of differences in throw caused by measurement obliquity on the calculation of SGR. We use the Chandon-1 well, resampled to every metre, to calculate V_{shale} of the succession and to construct juxtaposition diagrams (Fig. 14a).

Our assessment shows that repeatability and obliquity errors have only a minor impact on the SGR calculation across SF2 (Fig. 14b and c), with the V_{shale} of the intervening succession playing a more significant role in the calculation. The interval of interest between H1 and H12 is characterised by high V_{shale} values (average = 50%). As a result, most offsets exhibit siltstone-shale or shale-shale juxtapositions (Fig. 14a). Despite some differences between repeat datasets, the mean values of SGR for H9 and H12 show negligible variations, with larger differences observed only locally over short distances (<500 m). This is important for assessing the juxtaposition windows of reservoir units, as the magnitude of these difference could be sufficient to enable across fault fluid flow. It also suggests that the use of population statistics are insufficient when assessing the location of leakage points using SGR analysis.

Obliquity datasets also demonstrate variations in SGR between horizons, but the differences between datasets for the same horizon are low (Fig. 14c). The abundance of shale-shale or sand-shale juxtapositions explain these low differences; however, it should be noted that the magnitude of difference between picks would be similar in more sand rich succsessions. This would cause SGR values to be more sensitive to uncertainties in throw as smaller changes in throw could push the SGR above or below the sealing threshold. Similarly, to the repeatability datasets, obliquity datasets likely show patches where changes in SGR between datasets are high. Indeed, local changes in throw observed on Figs. 9, 11 and 12 support this suggestion. It is beyond the scope of this

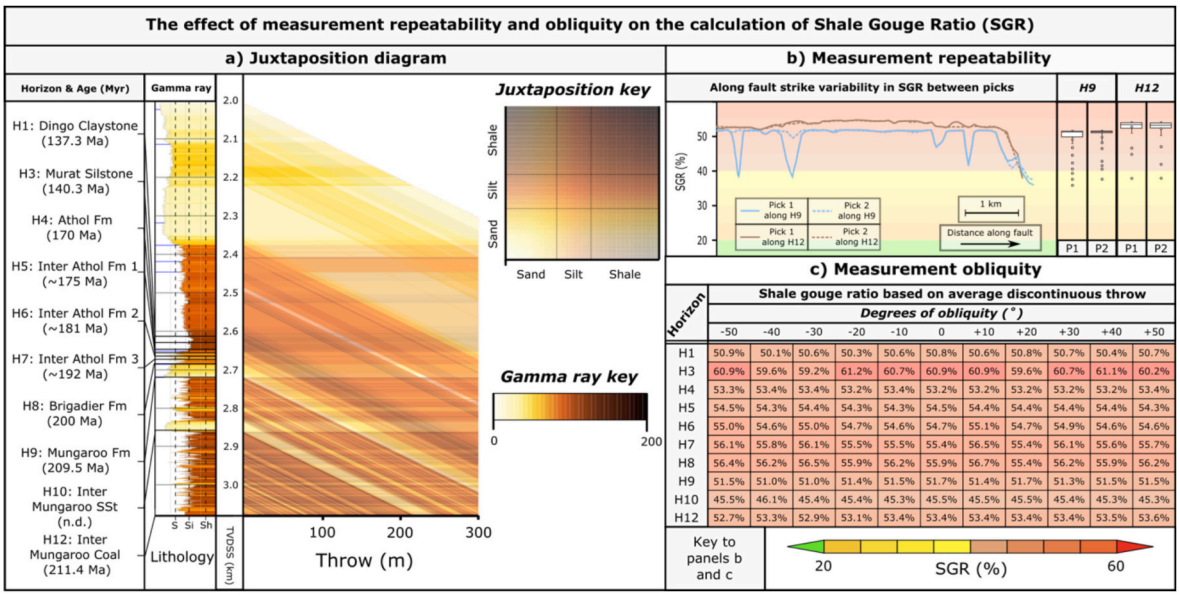

Fig. 14. The effect of repeatability and obliquity on the estimation of shale gouge ratio for fault transmissivity studied. Note how for this fault all values are above the sealing threshold, and the effect of repeatability and obliquity related errors are only locally important.

study to explicity explore the effect of obliquity and repeatability on the transmissivity of reservoir bounding faults; however, our results suggest that repeatability and obliquity errors in throw could cause a difference in the location and sealing potential of juxtaposition windows.

5.2. Throw and slip on faults over time using discontinuous and continuous deformation

When sediment accumulation rate exceeds fault throw rate, comparing the difference in throw or slip across two age-constrained horizons allows for the investigation of long-term throw or slip rate, which has applications for understanding fault growth (Marsh et al., 2010; Osagiede et al., 2014; Pan et al., 2022), strain partitioning between genetically related fault systems (Meyer et al., 2002; Cowie et al., 2005; Marsh et al., 2010) and using slip rates to understand and quantify seismic hazard (Nicol et al., 2005; Gambino et al., 2022).

In our study, we focus on the impact of measurement obliquity uncertainty on throw and slip rate across SF2 using multiple age-constrained horizons. Repeat picks were limited to Horizons H9 and H12, restricting our examination of the effect of repeatability on temporal slip-rate evolution, but enabling comparison of repeatability and obliquity errors for the 211.4 to 209.5 Ma period (Fig. 15). We calculate throw- and slip-rate using the continuous portion of the deformation, to account for any strain accommodated by near-fault deformation (e.g.,

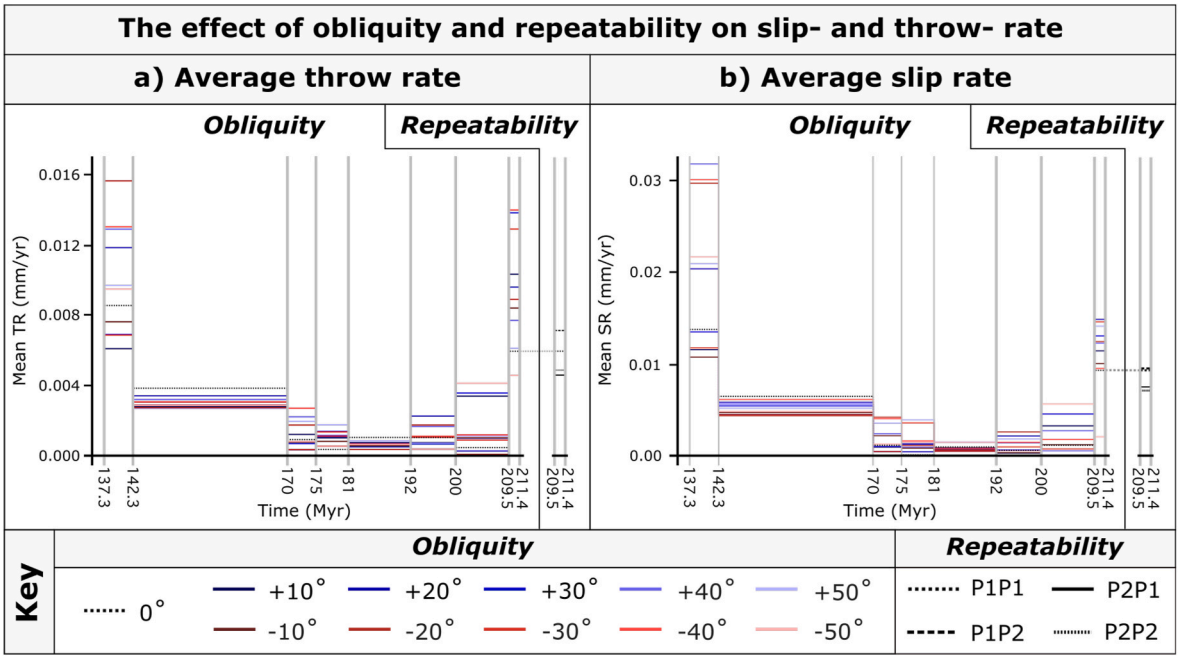

Fig. 15. The effect of repeatability and obliquity on the throw- and slip-rate of SF3 over time. Obliquity errors exceed repeatability errors for both mean throw- and slip-rate, and the effect of obliquity varies between time periods. P1 and P2 relates to the first and second pick across a given horizon, with the first value relating to H12 and the latter to H9. I.e., P1P2 relates to slip rate calculated using the 1st pick across H12 and the second pick across H9.

monocline formation). We take the difference in throw between each horizon, and divide this by the time period between the two horizons using the following equations:

$$\frac{throw_{H2} - throw_{H1}}{Age_{H2} - Age_{H1}}$$

$$\frac{Displacement_{H2} - Displacement_{H1}}{Age_{H2} - Age_{H1}}$$

Where H1 is the shallower horizon, and H2 the deeper horizon across the time-period of interest. Whereas uncertainties exist in the age of horizons, we do not consider these uncertainties here as they affect each dataset equally. Additionally, using the same horizon for each obliquity pick eliminates uncertainty introduced by mapping different reflections of potentially different ages.

Repeatability (211.4 to 209.5 Ma): Uncertainty in throw and slip rate, obtained from repeat picks, is influenced by the picks used and along-strike variations in fault properties (Figs. 15 and 16). Four pick combinations were analysed, resulting in mean throw rates ranging from 0.0045 to 0.0071 mm/yr. The percentage difference of these values (−14%–26%) exceed the repeatability of throw extracted from the continuous cut-off analysis. Mean slip rates ranged from 0.0071 to 0.0095 mm/yr. Unlike throw rates, no correlation was observed between picks and mean slip rates, with the greatest difference occurring where horizon picks from the same interpretation session were used. The difference in behaviour between throw and slip rates indicates that whereas throw was consistently lower for pick 1 when compared to pick 2, the same trend does not hold for heave. Along the fault, the slip rate profile showed similar shapes for all pick combinations, but subtle differences were observed, highlighting locations that were more susceptible to repeatability errors. Therefore, in cases with low to modest difference in slip (average 11 m) between horizons, the shape and magnitude of the slip profile may be influenced by repeatability errors.

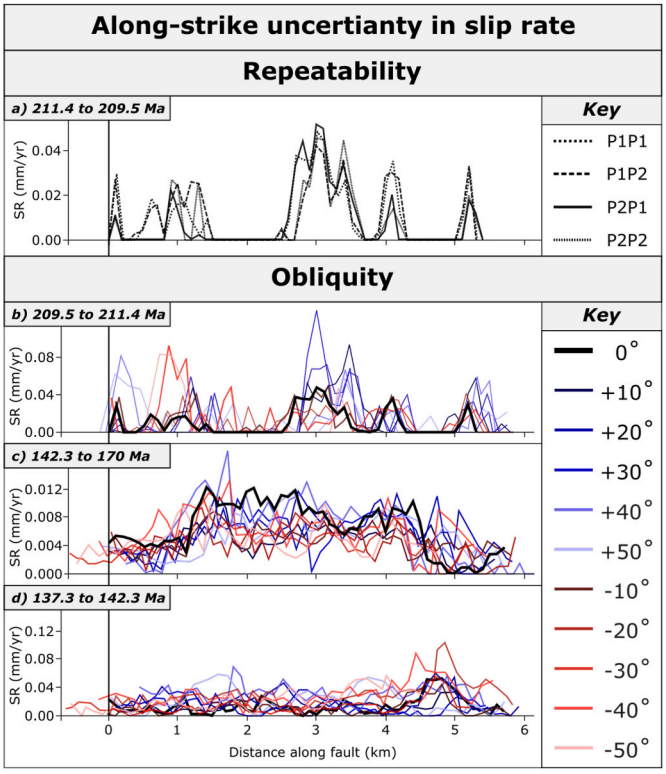

Fig. 16. The effect of repeatability and obliquity on the throw- and slip-rate evolution of SF3. Note how the shape of the profile differs between time periods, and between different measurement obliquities within that time period.

Obliquity: The errors for throw and slip rates due to measurement obliquity exceed the repeatability errors for datasets (Figs. 15 and 16). Measurement obliquity can affect the estimates of mean throw and slip rates, as compared to data collected from a strike-perpendicular transect (Fig. 15). From 211.4 to 209.5 Ma, throw rates extracted from oblique transects ranged from 0.0045 to 0.0140 mm/yr (absolute errors ranging from 3 to 135%), with only the −50° dataset having a lower throw rate than the strike-perpendicular transect. For the same time period, mean slip rates range from 0.0095 to 0.0149 mm/yr (absolute errors ranging from 1 to 60%), with all datasets (except −50°) exceeding the strike-perpendicular transect. The effect of measurement obliquity varies through time and differed between throw- and slip-rate (Fig. 15). Oblique sampling resulted in over- or under-estimations of throw and slip rates, with no consistent pattern observed. Along-fault profiles were sensitive to both repeatability and obliquity errors, altering the location and magnitude of throw- and slip-rate minima and maxima (Fig. 16). The influence of measurement obliquity on slip-rate profiles depended more on the time period measured (i.e., which pair of horizons were sampled) than the magnitude of measurement obliquity. Overall, even modest measurement obliquities (i.e., ±20°), and to a lesser extent repeatability errors, led to large differences in fault length inferred from along-fault profiles and throw- or slip-rate used to calculate fault-based seismic hazard.

6. Discussion

6.1. Impact and mitigation of fault interpretation uncertainty

6.1.1. Interpretation repeatability

From our study, we conclude that where the quality of the seismic imagery is good and the data are extracted by an interpreter with a similar level of experience, the repeatability of extracted data will depend on the fault property being extracted, and the fault and horizon that the data is extracted from (Table 1). Throw was found to be least sensitive to repeatability errors (7%), with heave (27%), displacement (16%) and dip (16%) showing greater sensitivity. Previous work has suggested that the interpretation of fault properties from low-displacement dyke-induced faults could be affected by measurement uncertainties of between ±5% (Magee and Jackson, 2020a) and ±10% (Magee et al., 2023). Our study highlights that this range is not sufficient to capture the uncertainty in heave (and therefore displacement and dip), particularly if multiple interpreters with greater subjective bias are involved.

Suggestions: Repeatability errors are difficult to quantify and will depend on the quality of the seismic image, the experience of the interpreter, and other human factors. As such the appropriate size of the error bars will differ from the values presented in this study. However, our study provides a first-pass parametric study of the influence of repeatability errors on the extraction of fault properties, suggesting errors >10% are to be expected, particularly in low-quality datasets or where low-displacement faults are present. Additionally, studies that rely on displacement as an input will likely show greater uncertainty compared to those that use throw as an input. Study specific error values could be obtained by undertaking repeat picks on a subset of the data.

6.2. Measurement obliquity

From our study, we conclude that the derived measurement obliquity broadly follows the theoretical trends (Fig. 3), but that the magnitude of the resulting error exceeds the theoretical values. The higher than expected errors may be due to 'non-geometrical' obliquity errors of the type discussed in Section 6.2. Our findings suggest that measurement obliquity should be limited, where possible, to ±20° around the orthogonal to the local fault strike.

However, it may not be practical to always interpret orthogonal to the local fault strike, for example when only 2D seismic datasets are

available, or when the fault strike is highly variable. For a fault that is highly sinuous, it would be time-consuming to construct numerous arbitrary lines orthogonal to differently orientated fault sections. In that case, additional steps would be required to ensure that the picks from differentialy orientated arbitrary lines are combined in a mathematically and geometrically appropriate way.

Suggestions: Measurement obliquity should not exceed ±20°, and where possible ±15°. This ensures that obliquity errors are minimised, whilst still ensuring that data is collected in a time-efficient manner. This rule is particularly important when continuous cut-offs are measured. Where it is not possible to reduce the measurement obliquity, results could be improved by 'correcting' heave, dip, and displacement values based on local strike calculated from measured cut-offs and the theoretical relationships outlined in Fig. 3. However, whilst this would decrease the overall errors, it cannot account for any non-geometrical errors in the dataset.

6.3. Interpreted cut-off type

Our work highlights that the interpreted cut-off type influences the magnitude of both repeatability and obliquity related errors (Tables 1, S7-14, Figs. 7–13). Greater uncertainty was observed where continuous cut-offs are included in the analysis, with the effect particularly clear when extracting heave (Table 1, Fig. 10).

Suggestions: The choice of interpreted cut-off type is often driven by study design. For example, assessing fault transmissivity necessitates discontinuous cut-offs to account for physical disconnections across the fault, while calculating long-term strain rate requires continuous cut-offs to accommodate non-discrete deformation. However, we found that the extraction of heave from fault cut-offs is particularly sensitive to both repeatability and obliquity errors and that the magnitude of error for the latter can greatly exceed theoretical values. Therefore, it may be better to use an average dip between two or more mapped horizons to calculate heave from the measured throw value. This will also reduce the effect of sample-specific measurement errors on the extraction of slip-rate.

6.4. Factors that control the magnitude of repeatability and non-geometrical obliquity errors

Our study suggests that the extraction of fault properties from cut-off data is strongly affected by the three elements of fault interpretation focused on in this study, and that these elements contribute to uncertainty in deriving interpretations from these data. Additionally, the effect of each element can vary both between faults and spatially along a single fault. During the work, we identified several additional factors that combine to increase, or decrease, the uncertainty at a given point along the fault, which are summarised below and in Fig. 17.

Our data suggests that the quality of the mapped reflection plays a large role in non-geometrical errors and low repeatability (Fig. 2a), as evidenced by certain horizons (e.g., H1) showing high errors (Table S2). Our findings thus agreed with previous studies, in that the quality of the seismic imegry, in particular the reflector strength, effects the reliability of the interpretation derived from the image (e.g., Alcalde et al., 2017;

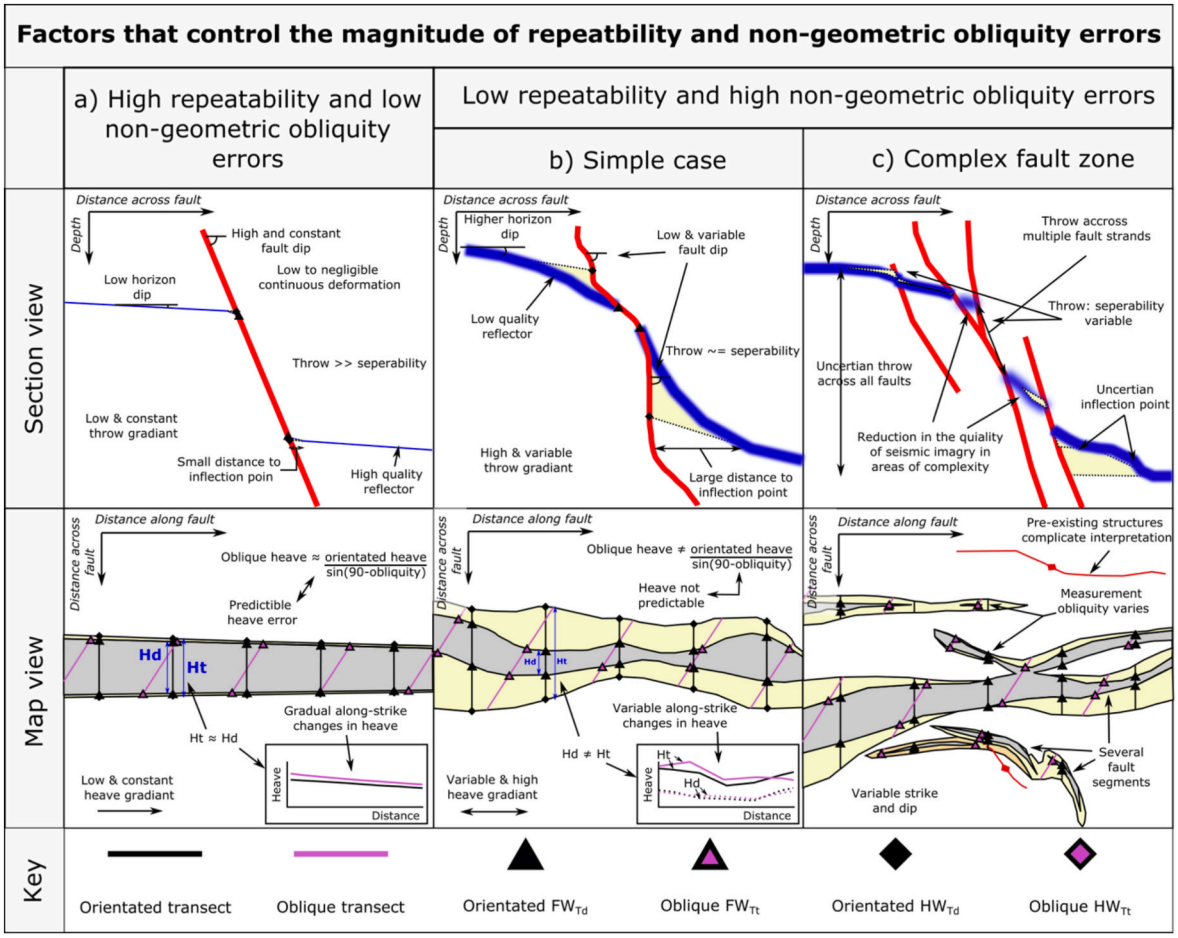

Fig. 17. Cartoons showing the factors that control the repeatability and magnitude of non-geometric obliquity errors. Examples are shown for a fault with high repeatability and low geometric errors (a), low repeatability and high geometric errors (b), and a more complex fault zone that is representative of relay zones observed in the seismic cube. See text for discussion of these factors.

Schaaf and Bond, 2019; Chellingsworth et al., 2015). The effect of the reflection quality does not influence each fault property equally, with heave (and thus displacement and dip) affected more than throw, due to the low regional dip (<3°) across the study area.

Our data shows that the uncertainty is affected by the size of the fault in terms of displacement or throw. There is greater uncertainty in areas of low throw, especially when close to or below the limit of seperability. When a large proportion of the deformation is taken up by folding (Fig. 17b), uncertainties are higher due to challenges in interpreting continuous cut-offs. These challenges are related to the variability of the horizon dip, the distance to the inflection point and the variability and magnitude of fault dip. Finally, uncertainties were particularly evident in complex fault zones (Fig. 17c), where the image quality may be more degraded and there may be challenges in interpreting deformation across multiple nearby fault strands. The factors shown in Fig. 17 indicate why there are along-strike and down-dip variations in the uncertainties, and therefore highlights that there may be local geometric variations in fault geometry that merit additional care and quantification of uncertainties.

7. Conclusions

Our study demonstrated that fault properties extracted from seismic reflection datasets are prone to three types of uncertainty: interpretation repeatability, measurement obliquity, and interpreted cut-off type. Obliquity related errors varies depending on the horizon and fault interpreted, the magnitude of obliquity, and the fault property measured. High errors occurred when obliquity exceeded ±20°, with throw showing lower percentage errors compared to heave across all datasets. Heave errors caused uncertainties in displacement and dip extraction, particularly in areas of low displacement. Repeatability errors were ~±10% for throw, and 13–23% for heave, with higher errors in areas of structural complexity or low seimic image quality. Measurement obliquity was not found to compound repeatability errors; however, interpreting continuous cut-offs increased uncertainty and error in extracted fault properties.

Measurement obliquity and interpretation repeatability had a minor effect on the calculation of shale gouge ratio (SGR) across SF2, however, significant errors were observed in local fault plane patches. The small difference in SGR is primarialy caused by the high Vshale content of the intervening succession. The magnitude of errors will be similar in reservoirs that have a greater sand content and are near the sealing threshold. In these cases, the fault might experience unexpected local cross-fault fluid flow, compromising for example carbon capture and storage facilities. Slip-rate extraction, which utilises continuous cut-offs, was strongly affected by both obliquity and repeatability errors. This could lead to over- or underestimation of slip-rate and differences in the interpretated slip-rate profile, impacting fault-based seismic hazard assessments, especially in low seismicity areas, and therefore the suitability for example of hosting a geological disposal facitlity for nuclear waste. These examples underline the importance of considering and mitigating obliquity and repeatbility errors when extracting fault data from seismic reflection datsets.

CRediT authorship contribution statement

Billy J. Andrews: Conceptualization, Data curation, Formal analysis, Investigation, Methodology, Writing – original draft, Writing – review & editing. **Zoë K. Mildon:** Conceptualization, Funding acquisition, Project administration, Supervision, Writing – original draft, Writing – review & editing. **Christopher A.L. Jackson:** Conceptualization, Methodology, Writing – review & editing. **Clare E. Bond:** Formal analysis, Supervision, Writing – review & editing.

Declaration of competing interest

The authors declare the following financial interests/personal relationships which may be considered as potential competing interests:

Zoe Mildon reports financial support was provided by University of Plymouth. Billy Andrews reports a relationship with University of Plymouth that includes: employment. No known conflicts of interest to delcare If there are other authors, they declare that they have no known competing financial interests or personal relationships that could have appeared to influence the work reported in this paper.

Data availability

Data will be made available on request.

Acknowledgements

We would like to thank DugInsight for the provision of an academic license for their software package.

We would like to thank Emma Miche and two anomalous reviewers for constructive feedback on the original version of the manuscipt

This work was supported by aUKRI Future Leaders Fellowship MR/T041994/1 (PI - Z. Mildon).

Appendix A. Supplementary data

Supplementary data to this article can be found online at https://doi.org/10.1016/j.jsg.2024.105158.

References

Alcalde, J., Bond, C.E., 2022. In: Bell, R., Iacopini, D., Vardy, M. (Eds.), Chapter 5 - Subjective Uncertainty and Biases: the Impact on Seismic Data Interpretation, Interpreting Subsurface Seismic Data. Elsevier, pp. 103–123. https://doi.org/10.1016/B978-0-12-818562-9.00002-9.

Alcalde, J., Bond, C.E., Johnson, G., Butler, R.W.H., Cooper, M.A., Ellis, J.F., 2017a. The importance of structural model availability on seismic interpretation. J. Struct. Geol. 97, 161–171. https://doi.org/10.1016/j.jsg.2017.03.003.

Alcalde, J., Bond, C.E., Johnson, G., Ellis, J.F., Butler, R.W.H., 2017b. Impact of seismic image quality on fault interpretation uncertainty. GSA Today (Geol. Soc. Am.). https://doi.org/10.1130/GSATG282A.1.

Allen, P.A., Allen, J.R., 2013. Basin Analysis: Principles and Application to Petroleum Play Assessment. John Wiley & Sons.

Amonette, J.E., Barr, J.L., Dobeck, L.M., Gullickson, K., Walsh, S.J., 2010. Spatiotemporal changes in CO2 emissions during the second ZERT injection, August–September 2008. Environ. Earth Sci. 60, 263–272. https://doi.org/10.1007/s12665-009-0402-0.

Andrews, B.J., Roberts, J.J., Shipton, Z.K., Bigi, S., Tartarello, M.C., Johnson, G., 2019. How do we see fractures? Quantifying subjective bias in fracture data collection. Solid Earth 10, 487–516. https://doi.org/10.5194/se-10-487-2019.

Bense, V.F., Gleeson, T., Loveless, S.E., Bour, O., Scibek, J., 2013. Fault zone hydrogeology. Earth Sci. Rev. 127, 171–192. https://doi.org/10.1016/j.earscirev.2013.09.008.

Bilal, A., McClay, K., 2022. Tectonic and stratigraphic evolution of the central Exmouth Plateau, NW shelf of Australia. Mar. Petrol. Geol. 136 https://doi.org/10.1016/j.marpetgeo.2021.105447.

Bilal, A., McClay, K., Scarselli, N., 2020. Fault-Scarp degradation in the central Exmouth Plateau, north west shelf, Australia. Geological Society, London, Special Publications 476, 231–257. https://doi.org/10.1144/SP476.11.

Black, M., McCormack, K.D., Elders, C., Robertson, D., 2017. Extensional fault evolution within the Exmouth sub-basin, north west shelf, Australia. Mar. Petrol. Geol. 85, 301–315. https://doi.org/10.1016/j.marpetgeo.2017.05.022.

Bond, C.E., 2015. Uncertainty in structural interpretation: lessons to be learnt. J. Struct. Geol. 74, 185–200. https://doi.org/10.1016/j.jsg.2015.03.003.

Bond, C.E., Gibbs, A.D., Shipton, Z.K., Jones, S., 2007. What do you think this is? "Conceptual uncertainty" in geoscience interpretation. GSA Today (Geol. Soc. Am.) 17, 4. https://doi.org/10.1130/GSAT01711A.1.

Bond, C.E., Lunn, R.J., Shipton, Z.K., Lunn, A.D., 2012. What makes an expert effective at interpreting seismic images? Geology 40, 75–78. https://doi.org/10.1130/G32375.1.

Brown, A.R., 2011. Interpretation of Three-Dimensional Seismic Data, seventh ed. American Association of Petroleum Geologists.

Chellingsworth, L., Bentley, M., Wynn, T., 2015. Human factors in seismic uncertainty — restoring a realistic uncertainty range. Interpretation 3, SQ21–SQ32. https://doi.org/10.1190/INT-2014-0203.1.

Childs, C., Manzocchi, T., Nicol, A., Walsh, J.J., Soden, A.M., Conneally, J.C., Delogkos, E., 2017. The relationship between normal drag, relay ramp aspect ratio

and fault zone structure. Geological Society, London, Special Publications 439, 355–372. https://doi.org/10.1144/SP439.16.
Childs, C., Manzocchi, T., Walsh, J.J., Bonson, C.G., Nicol, A., Schöpfer, M.P.J., 2009. A geometric model of fault zone and fault rock thickness variations. J. Struct. Geol. 31, 117–127. https://doi.org/10.1016/j.jsg.2008.08.009.
Choi, J.-H., Edwards, P., Ko, K., Kim, Y.-S., 2016. Definition and classification of fault damage zones: a review and a new methodological approach. Earth Sci. Rev. 152, 70–87. https://doi.org/10.1016/j.earscirev.2015.11.006.
Connor, C.B., Chapman, N.A., Connor, L.J., 2009. Volcanic and Tectonic Hazard Assessment for Nuclear Facilities. Cambridge University Press.
Cowie, P.A., Underhill, J.R., Behn, M.D., Lin, J., Gill, C.E., 2005. Spatio-temporal evolution of strain accumulation derived from multi-scale observations of Late Jurassic rifting in the northern North Sea: a critical test of models for lithospheric extension. Earth Planet Sci. Lett. 234, 401–419. https://doi.org/10.1016/j.epsl.2005.01.039.
Delogkos, E., Manzocchi, T., Childs, C., Sachanidis, C., Barbas, T., Schöpfer, M.P.J., Chatzipetros, A., Pavlides, S., Walsh, J.J., 2017. Throw partitioning across normal fault zones in the Ptolemais Basin, Greece. Geological Society, London, Special Publications 439, 333–353. https://doi.org/10.1144/SP439.19.
Delogkos, E., Saqab, M.M., Walsh, J.J., Roche, V., Childs, C., 2020. Throw variations and strain partitioning associated with fault-bend folding along normal faults. Solid Earth 11, 935–945. https://doi.org/10.5194/se-11-935-2020.
Direen, N.G., Stagg, H.M.J., Symonds, P.A., Colwell, J.B., 2008. Architecture of volcanic rifted margins: new insights from the Exmouth – gascoyne margin, Western Australia. Aust. J. Earth Sci. 55, 341–363. https://doi.org/10.1080/08120090701769472.
Faleide, T.S., Braathen, A., Lecomte, I., Mulrooney, M.J., Midtkandal, I., Bugge, A.J., Planke, S., 2021. Impacts of seismic resolution on fault interpretation: insights from seismic modelling. Tectonophysics 816, 229008. https://doi.org/10.1016/j.tecto.2021.229008.
Fenton, C.H., Adams, J., Halchuk, S., 2006. Seismic hazards assessment for radioactive waste disposal sites in regions of low seismic activity. Geotech. Geol. Eng. 24, 579–592. https://doi.org/10.1007/s10706-005-1148-4.
Frodeman, R., 1995. Geological reasoning: geology as an interpretive and historical science. Geol. Soc. Am. Bull. 107 (2), 960–968. https://doi.org/10.1130/0016-7606(1995)107<0960:GRGAAI>2.3.CO.
Gambino, S., Barreca, G., Gross, F., Monaco, C., Gutscher, M.-A., Alsop, G.I., 2022. Assessing the rate of crustal extension by 2D sequential restoration analysis: a case study from the active portion of the Malta Escarpment. Basin Res. 34, 321–341. https://doi.org/10.1111/bre.12621.
Gartrell, A., Torres, J., Dixon, M., Keep, M., Gartrell, A., Torres, J., Dixon, M., Keep, M., 2016. Mesozoic rift onset and its impact on the sequence stratigraphic architecture of the Northern Carnarvon Basin. The APPEA Journal 56, 143–158. https://doi.org/10.1071/AJ15012.
Gibson, R.G., Bentham, P.A., 2003. Use of fault-seal analysis in understanding petroleum migration in a complexly faulted anticlinal trap, Columbus Basin, offshore Trinidad. AAPG (Am. Assoc. Pet. Geol.) Bull. 87, 465–478. https://doi.org/10.1306/08010201132.
Goodman, S.N., 2016. Aligning statistical and scientific reasoning. Science 352, 1180–1181. https://doi.org/10.1126/science.aaf5406.
IPCC, 2005. Carbon Dioxide Capture and Storage. Cambridge University Press, Cambridge, UK.
Jackson, C.A.-L., Rotevatn, A., 2013. 3D seismic analysis of the structure and evolution of a salt-influenced normal fault zone: a test of competing fault growth models. J. Struct. Geol. 54, 215–234. https://doi.org/10.1016/j.jsg.2013.06.012.
Karner, G.D., Driscoll, N.W., 1999. In: MacNiocall, C., Ryan, P. (Eds.), Style, Timing and Distribution of Tectonic Deformation across the Exmouth Plateau, Northwest Australia, Determined from Stratal Architecture and Quantitative Basin Modelling, Continental Tectonics, Proceedings of the Ocean Drilling Program. Geological Society of London, London, UK, pp. 271–311. https://doi.org/10.2973/odp.proc.sr.122.1992.
Klusman, R.W., 2003. A geochemical perspective and assessment of leakage potential for a mature carbon dioxide–enhanced oil recovery project and as a prototype for carbon dioxide sequestration; Rangely field, Colorado. AAPG (Am. Assoc. Pet. Geol.) Bull. 87, 1485–1507. https://doi.org/10.1306/04220302032.
Lathrop, B.A., Jackson, C.A.-L., Bell, R.E., Rotevatn, A., 2021. Normal Fault kinematics and the role of lateral tip retreat: an example from offshore NW Australia. Tectonics 40, e2020TC006631. https://doi.org/10.1029/2020TC006631.
Magee, C., Jackson, C.A.-L., 2020a. Can we relate the surface expression of dike-induced normal faults to subsurface dike geometry? Geology 49, 366–371. https://doi.org/10.1130/G48171.1.
Magee, C., Jackson, C.A.-L., 2020b. Seismic reflection data reveal the 3D structure of the newly discovered Exmouth Dyke Swarm, offshore NW Australia. Solid Earth 11, 579–606. https://doi.org/10.5194/se-11-579-2020.
Magee, C., Love, V., Fayez, K., Andrews, B., Rivas-Dorado, S., Jackson, C., Orlov, C., Bramham, E., 2023. Quantifying dyke-induced graben and dyke structure using 3D seismic reflection data and the role of interpretation bias. Τεκτονικα 1, 32–53. https://doi.org/10.55575/tektonika2023.1.2.25.
Marsh, N., Imber, J., Holdsworth, R.E., Brockbank, P., Ringrose, P., 2010. The structural evolution of the Halten Terrace, offshore Mid-Norway: extensional fault growth and strain localisation in a multi-layer brittle–ductile system. Basin Res. 22, 195–214. https://doi.org/10.1111/j.1365-2117.2009.00404.x.
Meyer, V., Nicol, A., Childs, C., Walsh, J.J., Watterson, J., 2002. Progressive localisation of strain during the evolution of a normal fault population. J. Struct. Geol. 24, 1215–1231. https://doi.org/10.1016/S0191-8141(01)00104-3.
Michie, E.A.H., Mulrooney, M.J., Braathen, A., 2021. Fault Interpretation Uncertainties using Seismic Data, and the Effectson Fault Seal Analysis: a Case Study from the Horda Platform, withImplications for CO_2 storage. preprint. Tectonic plate interactions, magma genesis, and lithosphere deformation at all scales/Structural geology and tectonics, rock physics, experimental deformation/Structural geology. https://doi.org/10.5194/se-2021-23.
Miocic, J.M., Johnson, G., Gilfillan, S.M.V., 2014. Fault seal analysis of a natural CO2 reservoir in the Southern North Sea. Energy Procedia, 12th International Conference on Greenhouse Gas Control Technologies, GHGT- 12 63, 3364–3370. https://doi.org/10.1016/j.egypro.2014.11.365.
Mörner, N.-A., 2013. Patterns in seismology and palaeoseismology, and their application in long-term hazard assessments – the Swedish case in view of nuclear waste management. Pattern Recognition in Physics 1, 75–89. https://doi.org/10.5194/prp-1-75-2013.
Nicol, A., Walsh, J., Berryman, K., Nodder, S., 2005. Growth of a normal fault by the accumulation of slip over millions of years. J. Struct. Geol. 27, 327–342. https://doi.org/10.1016/j.jsg.2004.09.002.
Osagiede, E.E., Duffy, O.B., Jackson, C.A.-L., Wrona, T., 2014. Quantifying the growth history of seismically imaged normal faults. J. Struct. Geol. 66, 382–399. https://doi.org/10.1016/j.jsg.2014.05.021.
Pan, S., Bell, R.E., Jackson, C.A.-L., Naliboff, J., 2021. Evolution of normal fault displacement and length as continental lithosphere stretches. Basin Res. 34, 121–140. https://doi.org/10.1111/bre.12613.
Pan, S., Naliboff, J., Bell, R., Jackson, C., 2022. Bridging spatiotemporal scales of normal fault growth during continental extension using high-resolution 3D numerical models. G-cubed 23, e2021GC010316. https://doi.org/10.1029/2021GC010316.
Paumard, V., Bourget, J., Payenberg, T., Ainsworth, R.B., George, A.D., Lang, S., Posamentier, H.W., Peyrot, D., 2018. Controls on shelf-margin architecture and sediment partitioning during a syn-rift to post-rift transition: insights from the Barrow Group (northern Carnarvon Basin, north west shelf, Australia). Earth Sci. Rev. 177, 643–677. https://doi.org/10.1016/j.earscirev.2017.11.026.
Pérez-Díaz, L., Alcalde, J., Bond, C.E., 2020. Introduction: handling uncertainty in the geosciences: identification, mitigation and communication. Solid Earth 11, 889–897. https://doi.org/10.5194/se-11-889-2020.
Reeve, M.T., Jackson, C.A.-L., Bell, R.E., Magee, C., Bastow, I.D., 2016. The stratigraphic record of prebreakup geodynamics: evidence from the Barrow Delta, offshore Northwest Australia. Tectonics 35, 1935–1968. https://doi.org/10.1002/2016TC004172.
Reeve, M.T., Magee, C., Bastow, I.D., McDermott, C., Jackson, C.A.-L., Bell, R.E., Prytulak, J., 2021. Nature of the cuvier abyssal plain crust, offshore NW Australia. J. Geol. Soc. 178 https://doi.org/10.1144/jgs2020-172 jgs2020-172.
Robb, M.S., Taylor, B., Goodliffe, A.M., 2005. Re-Examination of the magnetic lineations of the gascoyne and cuvier abyssal plains, off NW Australia. Geophys. J. Int. 163, 42–55. https://doi.org/10.1111/j.1365-246X.2005.02727.x.
Robledo Carvajal, F., Butler, R.W.H., Bond, C.E., 2023. Mapping faults in 3D seismic data – why the method matters. J. Struct. Geol. 104976 https://doi.org/10.1016/j.jsg.2023.104976.
Roche, V., Camanni, G., Childs, C., Manzocchi, T., Walsh, J., Conneally, J., Saqab, M.M., Delogkos, E., 2021. Variability in the three-dimensional geometry of segmented normal fault surfaces. Earth Sci. Rev. 216, 103523 https://doi.org/10.1016/j.earscirev.2021.103523.
Rodríguez-Salgado, P., Childs, C., Shannon, P.M., Walsh, J.J., 2023. Influence of basement fabrics on fault reactivation during rifting and inversion: a case study from the Celtic Sea basins, offshore Ireland. J. Geol. Soc. 180, jgs2022–j2024. https://doi.org/10.1144/jgs2022-024.
Schaaf, A., Bond, C.E., 2019. Quantification of uncertainty in 3-D seismic interpretation: implications for deterministic and stochastic geomodeling and machine learning. Solid Earth 10, 1049–1061. https://doi.org/10.5194/se-10-1049-2019.
Shipton, Z.K., Cowie, P.A., 2003. A conceptual model for the origin of fault damage zone structures in high-porosity sandstone. J. Struct. Geol. 25, 333–344. https://doi.org/10.1016/S0191-8141(02)00037-8.
Shipton, Z.K., Roberts, J.J., Comrie, E.L., Kremer, Y., Lunn, R.J., Caine, J.S., 2020. Fault fictions: systematic biases in the conceptualization of fault-zone architecture. Geological Society, London, Special Publications 496, 125–143. https://doi.org/10.1144/SP496-2018-161.
Stagg, H., Alcock, M., Bernardel, G., Moore, A., Symonds, P., Exon, N., 2004. Geological Framework of the Outer Exmouth Plateau and Adjacent Ocean Basins. Geoscience Australia.
Steventon, M.J., Jackson, C.A.-L., Hall, M., Ireland, M.T., Munafo, M., Roberts, K.J., 2022. Reproducibility in subsurface geoscience. Earth Science, Systems and Society 2, 10051. https://doi.org/10.3389/esss.2022.10051.
Tannert, C., Elvers, H.-D., Jandrig, B., 2007. The ethics of uncertainty. EMBO Rep. 8, 885–974. https://doi.org/10.1038/sj.embor.7401072.
Taylor, S.K., Nicol, A., Walsh, J.J., 2008. Displacement loss on growth faults due to sediment compaction. J. Struct. Geol. 30, 394–405. https://doi.org/10.1016/j.jsg.2007.11.006.
Terzaghi, R.D., 1965. Sources of error in joint surveys. Geotechnique 15, 287–304. https://doi.org/10.1680/geot.1965.15.3.287.
Tindale, K., Newell, N., Keall, J., Smith, N., 1998. Abstract: Structural Evolution and Charge History of the Exmouth Sub-Basin Northern Carnarvon Basin, Offshore Western Australia.
Watkins, H., Bond, C.E., Healy, D., Butler, R.W.H., 2015. Appraisal of fracture sampling methods and a new workflow to characterise heterogeneous fracture networks at outcrop. J. Struct. Geol. 72, 67–82. https://doi.org/10.1016/j.jsg.2015.02.001.

Yang, X.-M., Elders, C., 2016. The mesozoic structural evolution of the gorgon platform, North Carnarvon basin, Australia. Aust. J. Earth Sci. 63, 755–770. https://doi.org/10.1080/08120099.2016.1243579.

Yielding, G., 2002. In: Koestler, A.G., Hunsdale, R. (Eds.), Shale Gouge Ratio — Calibration by Geohistory, Norwegian Petroleum Society Special Publications, Hydrocarbon Seal Quantification. Elsevier, pp. 1–15. https://doi.org/10.1016/S0928-8937(02)80003-0.

Yielding, G., Lykakis, N., Underhill, J.R., 2011. The role of stratigraphic juxtaposition for seal integrity in proven CO2 fault-bound traps of the Southern North Sea. Petrol. Geosci. 17, 193–203. https://doi.org/10.1144/1354-0793/10-026.